

Constraints on Dark Energy and Modified Gravity Models from Fast Radio Bursts and Late-Time Geometric Probes

Bruno W. N. Ribeiro ^{a,1} Lázaro L. Sales ^{b,a} K. E. L. de Farias ^a
Raiff H. Santos ^a Rafael A. Batista ^a Amílcar R. Queiroz ^a

^aUniversidade Federal de Campina Grande,
R. Aprígio Veloso 882, Bairro Universitário, 58429-900, Campina Grande, PB, Brazil

^bUniversidade do Estado do Rio Grande do Norte,
Av. Prof. Antônio Campos, Pres. Costa e Silva, 59610-210, Mossoró, RN, Brazil

E-mail: brunoweslley92@gmail.com

Abstract. We investigate the impact of 104 localized FRBs on cosmological parameter estimation when combined with three established late-time probes: Cosmic Chronometers (CC), Type Ia Supernovae (SNe), and Baryon Acoustic Oscillations (BAO). By performing a Bayesian analysis of three dark energy models (Λ CDM, w CDM, and CPL) and three viable $f(R)$ gravity scenarios — the Appleby–Battye (AB), Hu–Sawicki (HS), and Starobinsky (ST) models —, we find that FRBs substantially improve the constraints on the baryon density Ω_b by 25%–43%, the Hubble constant H_0 by 12%–35%, and the SNe absolute magnitude M_B by 10%–32%. Constraints on dark energy parameters show more modest improvements, with w improving by $\sim 9\%$ in w CDM and (w_0, w_a) improving by $\sim (8, 22)\%$ in the CPL parametrization. Modified gravity parameters remain weakly constrained, with improvements of only 6%–15%, indicating the limited sensitivity of current datasets to departures from Λ CDM. The Figure of Merit analysis shows overall improvements ranging from $\sim 48\%$ (Λ CDM) to $\sim 91\%$ (CPL), driven by enhanced precision in the (H_0, Ω_b) plane. Model comparison reveals moderate statistical preference for extensions beyond Λ CDM: AIC strongly favors w CDM, CPL, HS, and ST with $\Delta\text{AIC} < -7$, and LRT yields $p \leq 0.004$, while BIC returns to positive evidence ($-3.2 < \Delta\text{BIC} < -2.7$). These results show that FRBs may be useful as a complementary probe, particularly for constraining Ω_b and alleviating key late-time degeneracies.

Contents

1	Introduction	2
2	Cosmological Background	3
2.1	Flat FLRW Universe	4
2.2	Distance Measures and Cosmological Observables	4
3	Fast Radio Bursts	5
3.1	Statistical Description of the DM Components	6
4	Cosmological Models	7
4.1	GR-Based Models	7
4.2	Modified Gravity: $f(R)$ Theories	8
4.2.1	General Framework	8
4.2.2	Viability conditions	9
4.2.3	Starobinsky regularization	10
4.2.4	Appleby-Battye	10
4.2.5	Hu-Sawicki	11
4.2.6	Starobinsky	11
5	Observational Datasets	11
6	Statistical Methodology	12
6.1	Numerical Implementation	13
6.2	Joint Likelihood	14
6.3	Figure of Merit	15
6.4	Model Selection Criteria	15
7	Results and discussions	16
7.1	Λ CDM	16
7.2	w CDM	17
7.3	CPL	19
7.4	Appleby-Battye	20
7.5	Hu-Sawicki	22
7.5.1	Starobinsky	23
7.6	FRB nuisance parameters	25
7.7	The Impact of FRBs	25
7.8	Model Comparison	26
8	Conclusion	27
A	$f(R)$ Background Dynamics	29
B	CC and FRB Catalogs	30
C	Interpolation Grid Validation	34

1 Introduction

The discovery of the late-time accelerated expansion of the Universe [1, 2] has established the cosmological constant Λ as the simplest explanation for dark energy. However, the Λ Cold Dark Matter (Λ CDM) paradigm faces profound theoretical challenges, such as the fine-tuning and cosmic coincidence problems [3]. More recently, this theoretical discomfort has been amplified by persistent observational tensions that threaten the internal consistency of the standard model. The most notable is the Hubble tension, a $4\text{--}6\sigma$ discrepancy between the H_0 value inferred from the Cosmic Microwave Background (CMB) under Λ CDM assumptions and direct local measurements obtained from type Ia Supernovae (SNe Ia) [4, 5]. This is accompanied by the S_8 tension, in which weak lensing and galaxy clustering surveys find a lower amplitude of matter fluctuations than predicted by Planck data [6]. These anomalies suggest that the standard model may be an incomplete description of the dark sector, motivating exploration of extensions beyond Λ CDM.

Within the General Relativity (GR) framework, a wide class of extensions has been proposed by relaxing the assumption of a cosmological constant. The simplest extension is the w CDM model, which assumes a constant equation of state (EoS) parameter $w \neq -1$, while more general parameterizations such as the Chevallier–Polarski–Linder (CPL) model allow for time-dependent EoS, describing dynamical dark energy [7, 8]. These models retain the geometrical structure of GR while extending the dark sector, and serve as natural frameworks for testing departures from Λ CDM while remaining within observationally well-tested gravitational theory.

Alternatively, theories of modified gravity based on $f(R)$ functions offer a geometrically motivated framework that reproduces accelerated expansion by modifying the gravitational sector itself, without introducing additional exotic components in the energy–momentum tensor. In these models, the Ricci scalar R in the Einstein–Hilbert action is replaced by a general function of R , effectively generating acceleration through higher-order curvature corrections rather than a dark energy fluid. Several viable $f(R)$ models, including those of Appleby & Battye [9], Hu & Sawicki [10], and Starobinsky [11], reproduce the observed cosmic acceleration while satisfying local gravity constraints and recovering GR in the appropriate limit, making them well-motivated targets for independent cosmological tests.

Late-time cosmology currently relies on a combination of geometrical probes, each sensitive to different aspects of the expansion history. Cosmic Chronometers (CC) provide direct measurements of the Hubble parameter through differential age evolution of galaxies, while SNe Ia act as standardizable candles tracing the luminosity distance. Baryon Acoustic Oscillations (BAO), in turn, offer a standard ruler that constrains both the angular diameter distance and the Hubble rate. Despite their success, these probes exhibit parameter degeneracies and limited sensitivity to specific components of the cosmic energy budget, particularly the baryonic sector, highlighting the need for additional independent observables.

Recently, in 2007, another astrophysical phenomenon was discovered by Lorimer et al. [12], the Fast Radio Bursts (FRBs), which are millisecond-duration radio transients of extragalactic origin [13] whose dispersion measure (DM) encodes information about the integrated free-electron content along the line of sight. Since the intergalactic medium (IGM) contribution to the DM scales with the baryon density and the expansion history, FRBs with known redshifts may provide a novel and independent cosmological probe, complementary to CC, SNe, and BAO. Recent observational programs such as CHIME/FRB [14] and ASKAP [15] has dramatically increased the rate of FRB detections, with several hundred events now localized to host galaxies [16–24]. Early studies have demonstrated the potential of FRBs to

constrain the cosmic baryon density and probe the distribution of ionized gas in the IGM [25]. However, current analyses remain limited by systematic uncertainties associated with host galaxy contributions and line-of-sight inhomogeneities. Since both dark energy and modified gravity models affect the background expansion history, they leave imprints on the DM– z relation, making FRBs a complementary probe with particular sensitivity to the baryonic sector and the expansion history, thus providing an independent consistency check on existing constraints.

Despite these advances, existing studies on FRBs have focused primarily on model-independent cosmographic analyses, Λ CDM constraints, Hubble-constant measurements, or individual dark energy extensions [25–30]. A comprehensive assessment that simultaneously addresses the impact on parameter degeneracies across multiple models, the propagation to derived cosmological quantities, modified-gravity scenarios, and model selection within a unified statistical framework remains lacking. In particular, it is unclear how FRBs affect the constraining power of joint late-time datasets and whether they provide sufficient discriminating power to favor extensions beyond Λ CDM when complexity penalties are properly accounted for.

In this work, we perform a systematic and unified investigation of the constraining power of FRBs when combined with traditional late-time probes, which introduces several methodological advances. We simultaneously analyze both dark energy and viable $f(R)$ modified gravity scenarios within a consistent Bayesian framework, quantify improvements on primary parameters and parameter degeneracies, and apply multiple complementary model selection criteria to assess statistical preference. Specifically, our main contributions are: (i) we perform joint Bayesian analyses for the Baseline (CC + SNe + BAO) and Baseline + FRB datasets across six cosmological models; (ii) we quantify the improvement in cosmological parameter constraints through the reduction of their uncertainties when FRBs are included; (iii) we assess the global impact of FRBs using the Figure of Merit (FoM) metric; and (iv) we evaluate the model selection using the Akaike (AIC) and Bayesian (BIC) information criteria, as well as the Likelihood Ratio Test (LRT).

This paper is organized as follows. Sec. 2 introduces the cosmological framework and the distance measures relevant for late-time probes. The FRB formalism, including the DM modeling and its statistical description, is presented in Sec. 3. In Sec. 4 we describe the cosmological models under consideration, encompassing both GR-based dark energy parametrizations and viable $f(R)$ modified gravity scenarios. The observational datasets and their respective systematics are detailed in Sec. 5. In Sec. 6, we present the statistical framework, including the Bayesian inference setup, prior choices, joint likelihood construction, numerical implementation, and MCMC sampling strategy, together with the Figure of Merit and model selection criteria adopted in this work. Our results and discussions are reported in Sec. 7, and a summary of our main conclusions in Sec. 8.

2 Cosmological Background

This section summarizes the theoretical framework underlying the cosmological observables used in this work. We begin by introducing the background dynamics of a spatially flat FLRW universe, followed by the definition of the distance measures that connect the expansion history to observations.

2.1 Flat FLRW Universe

We assume a spatially flat, homogeneous and isotropic universe described by the Friedmann-Lemaître-Robertson-Walker (FLRW) metric:

$$ds^2 = -dt^2 + a^2(t) [dr^2 + r^2 d\Omega^2], \quad (2.1)$$

where $a(t)$ is the scale factor normalized to $a_0 = 1$ today, and $H(t) \equiv \dot{a}/a$ is the Hubble parameter with present value H_0 . The redshift z is related to the scale factor by $1+z = 1/a(t)$.

The energy content of the universe is described by a perfect fluid with energy-momentum tensor:

$$T_{\mu\nu} = (\rho + p) u_\mu u_\nu + p g_{\mu\nu}, \quad (2.2)$$

where ρ is the energy density, p is the pressure, and u^μ is the four-velocity of the fluid. The component i is characterized by an equation of state (EoS) $w_i \equiv p_i/\rho_i$, whose energy density evolves as

$$\rho_i(z) = \rho_{i,0} (1+z)^{3(1+w_i)}, \quad (2.3)$$

for constant w_i . The case $w_i = 0$ corresponds to pressureless nonrelativistic matter, such as baryons and cold dark matter, for which $\rho_m \propto (1+z)^3$. On the other hand, $w_i = -1$ corresponds to a cosmological constant, with $\rho_\Lambda = \text{const}$. The density parameter is defined as $\Omega_i \equiv \rho_{i,0}/\rho_{\text{crit},0}$, where $\rho_{\text{crit},0} = 3H_0^2/8\pi G$ is the critical density today.

2.2 Distance Measures and Cosmological Observables

In a spatially flat FLRW universe, the distance measures relevant to late-time cosmology are derived from the comoving distance $D_C(z)$, defined as

$$D_C(z) = c \int_0^z \frac{dz'}{H(z')}, \quad (2.4)$$

which encodes the expansion history through the Hubble rate. The luminosity distance D_L and angular diameter distance D_A follow directly as

$$D_L(z) = (1+z) D_C(z), \quad D_A(z) = \frac{D_C(z)}{1+z}, \quad (2.5)$$

where D_L accounts for expansion-induced energy loss and time dilation, while D_A relates the transverse size of a source to its observed angular extent. The $(1+z)$ factor relating D_L and D_A reflects the Etherington reciprocity relation [31], which holds in any metric theory of gravity for photons traveling on null geodesics.

These two quantities can be obtained by measurement of Supernovae Ia in the case of $D_L(z)$, and for $D_A(z)$, it is provided by the baryon acoustic oscillations. The brightness of SNe Ia is used as a standard candle, and it depends on the luminosity distance to the source. The predicted apparent magnitude in the rest-frame B -band at redshift z is related to the distance modulus μ_B by

$$m_B(z) = \mu_B(z) + M_B, \quad \mu_B(z) \equiv 5 \log_{10} \left[\frac{D_L(z)}{\text{Mpc}} \right] + 25, \quad (2.6)$$

where M_B is the absolute magnitude in the rest-frame B -band, treated as a free nuisance parameter.

The BAO feature is calibrated against the sound horizon at the drag epoch, r_d , which sets the characteristic comoving scale imprinted by acoustic oscillations in the pre-recombination plasma. This quantity is defined as the total comoving distance travelled by sound waves from the Big Bang until the moment baryons kinematically decouple from the photon fluid at redshift $z_d \approx 1060$, and it is expressed as:

$$r_d = \int_{z_d}^{\infty} \frac{c_s(z)}{H(z)} dz, \quad (2.7)$$

where $c_s(z)$ denotes the adiabatic sound speed in the coupled photon-baryon fluid and z_d marks the drag epoch, at which the photon pressure becomes dynamically relevant, and the baryonic component effectively freezes out of the acoustic oscillations.

Under the assumption of standard early-universe physics, the resulting fit takes the form [32]

$$r_d = 147.05 \left(\frac{\Omega_b h^2}{0.02236} \right)^{-0.13} \left(\frac{\Omega_m h^2}{0.1432} \right)^{-0.23} \left(\frac{N_{\text{eff}}}{3.04} \right)^{-0.1} \text{ Mpc}, \quad (2.8)$$

where the pivot values correspond to the Planck best-fit cosmology [33], $h \equiv \frac{H_0}{100 \text{ km s}^{-1} \text{ Mpc}^{-1}}$, and N_{eff} accounts for neutrino species that remain ultrarelativistic throughout the pre-recombination epoch. In this work, we fix $N_{\text{eff}} = 3.046$, corresponding to the standard prediction from non-instantaneous neutrino decoupling in the early universe.

3 Fast Radio Bursts

The key observable of an FRB is its Dispersion Measure, which arises from the frequency-dependent time delay experienced by the radio signal as it propagates through ionized plasma [34]:

$$\Delta t \propto \left(\frac{1}{\nu_{\text{lo}}^2} - \frac{1}{\nu_{\text{hi}}^2} \right) \text{DM}, \quad (3.1)$$

where ν_{lo} and ν_{hi} denote the lower and upper frequencies of the signal. The DM corresponds to the integrated column density of free electrons along the line of sight,

$$\text{DM} = \int \frac{n_e(z)}{1+z} dl, \quad (3.2)$$

where the factor $(1+z)^{-1}$ accounts for cosmological time dilation.

The observed DM can be decomposed into distinct physical contributions:

$$\text{DM}_{\text{obs}}(z) = \text{DM}_{\text{MW}} + \text{DM}_{\text{IGM}} + \frac{\text{DM}_{\text{host}}}{1+z}, \quad (3.3)$$

where $\text{DM}_{\text{MW}} = \text{DM}_{\text{MW,ISM}} + \text{DM}_{\text{MW,halo}}$ accounts for the Galactic interstellar medium and halo, DM_{IGM} corresponds to the intergalactic medium, and DM_{host} represents the host galaxy contribution. The extragalactic dispersion measure is obtained by subtracting the Galactic contribution from the observed signal, as

$$\begin{aligned} \text{DM}_{\text{ext}}(z) &\equiv \text{DM}_{\text{obs}}(z) - \text{DM}_{\text{MW}} \\ &= \text{DM}_{\text{IGM}} + \frac{\text{DM}_{\text{host}}}{1+z}. \end{aligned} \quad (3.4)$$

where the Galactic contribution is estimated using the electron density model NE2001 [35].

The cosmological information encoded in FRBs enters through the contribution of the IGM. Its ensemble average is given by the Macquart relation [28],

$$\langle \text{DM}_{\text{IGM}}(z) \rangle = \frac{3c f_{\text{IGM}} \Omega_b H_0^2}{8\pi G m_p} \int_0^z \frac{(1+z') x_e(z')}{H(z')} dz', \quad (3.5)$$

where f_{IGM} denotes the fraction of baryons residing in the IGM, m_p is the proton mass, and $x_e(z)$ is the free-electron fraction per baryon, given by

$$x_e(z) = Y_H x_{e,H}(z) + \frac{1}{2} Y_{\text{He}} x_{e,\text{He}}(z), \quad (3.6)$$

with hydrogen and helium mass fractions $Y_H = 3/4$ and $Y_{\text{He}} = 1/4$.

Observational and numerical studies regarding the baryon fraction in the IGM suggest that the value of f_{IGM} lies within the range $0.7 \lesssim f_{\text{IGM}} \lesssim 0.95$ [27, 29, 36–39], reflecting uncertainties in the baryon distribution between collapsed structures and the diffuse IGM. In this work, we adopt $f_{\text{IGM}} = 0.83$, a representative value consistent with recent observational and simulation-based estimates [29, 36, 38]. In addition, since hydrogen and helium are fully ionized at $z < 3$ [40, 41], we take $x_{e,H} = x_{e,\text{He}} = 1$, yielding $x_e = 7/8$.

3.1 Statistical Description of the DM Components

The IGM contribution to DM_{ext} is inherently stochastic due to the inhomogeneous distribution of baryons in the cosmic large-scale structure. The DM accumulated along a given line of sight traces the integrated column density of free electrons and is therefore sensitive to density fluctuations along different paths.

Based on semi-analytic models and hydrodynamical simulations, the distribution of DM_{IGM} at fixed redshift is approximately Gaussian around its mean, with non-Gaussian tails arising from rare intersections with dense structures, such as galaxy groups and massive halos, along the line of sight [28, 42–44]. More accurate descriptions of the IGM scatter have been proposed, which include quasi-log-normal profiles [42] and simulation-calibrated templates [43]. However, these non-Gaussian corrections become significant only at low redshift ($z \lesssim 0.1$), where the small number of intersected halos leads to a strongly asymmetric DM distribution, and their impact on parameter inference is negligible for the sample sizes currently available [44]. We therefore adopt a truncated Gaussian approximation as an effective description of the IGM scatter, which captures the dominant statistical uncertainty relevant for the present catalog of 104 FRBs, consistent with the approach adopted in several recent FRB cosmology analyses [28, 44].

The corresponding probability distribution is written

$$P_{\text{IGM}}(\text{DM}_{\text{IGM}} | z) = \frac{1}{\mathcal{N}(z)} \frac{1}{\sqrt{2\pi} \sigma_{\text{IGM}}(z)} \exp \left[-\frac{(\text{DM}_{\text{IGM}} - \langle \text{DM}_{\text{IGM}}(z) \rangle)^2}{2\sigma_{\text{IGM}}^2(z)} \right] \Theta(\text{DM}_{\text{IGM}}), \quad (3.7)$$

where $\Theta(x) = 1$ if $x \geq 0$ and $\Theta(x) = 0$ otherwise is the Heaviside step function enforcing the physical constraint $\text{DM}_{\text{IGM}} \geq 0$, and $\mathcal{N}(z)$ is the normalization factor of the truncated distribution,

$$\mathcal{N}(z) = \frac{1}{2} \left[1 + \text{erf} \left(\frac{\langle \text{DM}_{\text{IGM}}(z) \rangle}{\sqrt{2} \sigma_{\text{IGM}}(z)} \right) \right], \quad (3.8)$$

where $\langle \text{DM}_{\text{IGM}}(z) \rangle$ is given by the Macquart relation, Eq. (3.5), and $\sigma_{\text{IGM}}(z)$ encodes the redshift-dependent scatter arising from line-of-sight fluctuations in the large-scale structure. This truncation eliminates the unphysical probability assigned to negative dispersion measures by a pure Gaussian. In practice, since $\langle \text{DM}_{\text{IGM}}(z) \rangle \gg \sigma_{\text{IGM}}(z)$ for most sources in our sample, $\mathcal{N}(z) \approx 1$ and the truncated distribution reduces to the standard Gaussian to high accuracy. Nevertheless, we adopt the truncated form for statistical consistency, as the correction becomes non-negligible for low-redshift FRBs where the mean-to-scatter ratio is smallest.

Following previous studies, we model this scatter empirically as a power law in redshift,

$$\sigma_{\text{IGM}}(z) = \sigma_0 z^\gamma, \quad (3.9)$$

where σ_0 and γ are coefficients calibrated from simulation-based estimates of dispersion measure fluctuations. In particular, we adopt $\sigma_0 = 173.8 \text{ pc cm}^{-3}$ and $\gamma = 0.4$, following [45], where this form is obtained from a power-law fit to numerical results describing the impact of large-scale structure on the IGM dispersion.

In contrast to the intergalactic component, the host-galaxy contribution DM_{host} arises from the local environment of the source and depends on several astrophysical factors, such as the galaxy morphology, inclination, star formation activity, and the location of the burst within the host. These effects introduce significant scatter and intrinsic asymmetry in the DM_{host} distribution. Motivated by cosmological hydrodynamical simulations, such as IllustrisTNG, which show that DM_{host} follows a log-normal profile across different redshifts and galaxy types [46], we model this contribution as

$$P_{\text{host}}(\text{DM}_{\text{host}}) = \frac{1}{\sqrt{2\pi} \sigma_{\text{host}} \text{DM}_{\text{host}}} \exp \left[-\frac{1}{2} \left(\frac{\ln \text{DM}_{\text{host}} - \mu}{\sigma_{\text{host}}} \right)^2 \right], \quad (3.10)$$

where e^μ is the median and σ_{host} is the logarithmic width, both treated as free nuisance parameters.

4 Cosmological Models

In this Section, we consider two classes of models that account for the late-time acceleration: the extensions within General Relativity based on dark energy parametrizations and modified theories of gravity that alter the geometric sector of the field equations.

4.1 GR-Based Models

Starting with the framework of GR, it is considered that the late-time accelerated expansion of the Universe is given by a dark energy component whose nature remains unknown. Hence, we consider Λ CDM, which is the cosmological standard model and two other extensions, w CDM and CPL parametrizations.

In the standard cosmological model, it is assumed a spatially flat universe filled with pressureless CDM and a cosmological constant Λ , which acts as a perfect fluid with EoS $w_\Lambda = -1$ and constant energy density $\rho_\Lambda = \Lambda/(8\pi G)$. Using Eq. (2.3), the Friedmann equation takes the form

$$H^2(z) = H_0^2 [\Omega_m(1+z)^3 + \Omega_\Lambda], \quad (4.1)$$

where Ω_m is the non-relativistic matter density parameter and $\Omega_\Lambda = 1 - \Omega_m$ is the dark energy density parameter.

The first extension of Λ CDM replaces the cosmological constant with a dark energy component characterized by a constant but free EoS $w \neq -1$. From Eq. (2.3), the dark energy density evolves as $\rho_{\text{de}}(z) \propto (1+z)^{3(1+w)}$, which reduces to a constant for $w = -1$. The Friedmann equation becomes

$$H^2(z) = H_0^2 \left[\Omega_m(1+z)^3 + (1 - \Omega_m)(1+z)^{3(1+w)} \right]. \quad (4.2)$$

The Λ CDM limit is exactly recovered for $w = -1$, while $w > -1$ ($w < -1$) corresponds to quintessence (phantom) dark energy.

The Chevallier–Polarski–Linder (CPL) parametrization [7, 8] provides a minimal and well-motivated extension by allowing w to vary with redshift:

$$w(z) = w_0 + w_a \frac{z}{1+z} = w_0 + w_a(1-a), \quad (4.3)$$

where $w_0 \equiv w(z=0)$ is the present-day value and $w_a \equiv -dw/da|_{a=1}$ quantifies the rate of change with the scale factor. This parametrization is well-behaved at all redshifts: it reduces to w_0 today and approaches the finite value $w_0 + w_a$ in the early universe ($z \rightarrow \infty$), avoiding the divergences present in some alternative forms. Substituting Eq. (4.3) into the continuity equation and integrating yields $\rho_{\text{de}}(z) \propto (1+z)^{3(1+w_0+w_a)} \exp[-3w_a z/(1+z)]$, giving the Friedmann equation:

$$H^2(z) = H_0^2 \left[\Omega_m(1+z)^3 + (1 - \Omega_m)(1+z)^{3(1+w_0+w_a)} e^{-3w_a z/(1+z)} \right]. \quad (4.4)$$

The Λ CDM and w CDM limits are recovered for $(w_0, w_a) = (-1, 0)$.

4.2 Modified Gravity: $f(R)$ Theories

As a representative class of modified gravity scenarios, we focus on $f(R)$ theories, where the Einstein–Hilbert action is generalized to a nonlinear function of the Ricci scalar. We briefly summarize the general formalism and the conditions required for cosmological viability.

4.2.1 General Framework

The modified Einstein–Hilbert action for $f(R)$ gravity [47, 48] reads

$$S = \int d^4x \sqrt{-g} \left[\frac{M_{\text{Pl}}^2}{2} f(R) + \mathcal{L}_m \right], \quad (4.5)$$

where $M_{\text{Pl}}^2 \equiv (8\pi G)^{-1}$ is the reduced Planck mass and \mathcal{L}_m is the matter Lagrangian density. Varying Eq. (4.5) with respect to the metric $g_{\mu\nu}$ yields the modified field equations:

$$f_{,R} R_{\mu\nu} - \frac{f}{2} g_{\mu\nu} - (\nabla_\mu \nabla_\nu - g_{\mu\nu} \square) f_{,R} = \frac{T_{\mu\nu}}{M_{\text{Pl}}^2}, \quad (4.6)$$

where $f_{,R} \equiv df/dR$, and $T_{\mu\nu}$ is the energy-momentum tensor of matter. Taking the trace of Eq. (4.6) gives:

$$R f_{,R} - 2f + 3 \square f_{,R} = \frac{T}{M_{\text{Pl}}^2}, \quad (4.7)$$

where $T \equiv T^\mu{}_\mu$. In a vacuum, Eq. (4.7) reduces to

$$R f_{,R} - 2f = 0, \quad (4.8)$$

whose positive real roots define the de Sitter vacuum solutions that underpin both the inflationary and the late-time accelerated expansion phases of the Universe. A necessary condition for the existence of physically acceptable de Sitter solutions is

$$\left. \frac{f_{,R}}{f_{,RR}} \right|_{R=R_*} > R_*, \quad (4.9)$$

where $f_{,RR} \equiv d^2 f/dR^2$ and R_* is a positive real root of Eq. (4.8). This condition ensures the stability of the de Sitter solution under perturbations. Moreover, it is closely related to the requirement that the effective scalar degree of freedom remains well-behaved. It plays a central role in selecting physically viable $f(R)$ models.

Considering the spatially flat FLRW metric in Eq. (2.1) and the perfect-fluid energy-momentum tensor in Eq. (2.2), the modified field equations (4.6) yield

$$3f_{,R}H^2 = \rho_m + \frac{Rf_{,R} - f}{2} - 3H\dot{f}_{,R}, \quad (4.10)$$

$$-2f_{,R}\dot{H} = \rho_m + \ddot{f}_{,R} - H\dot{f}_{,R}, \quad (4.11)$$

where dots denote derivatives with respect to cosmic time. Radiation is neglected since we focus on the late-time evolution $z \ll z_{\text{eq}} \simeq 3400$, where $\rho_r(1+z) \ll \rho_m$. The Ricci scalar is related to H through $R = 6(\dot{H} + 2H^2)$. Together with Eq. (4.6), these form a closed system for the background evolution, which reduces to the standard Friedmann equations for $f(R) = R - 2\Lambda$.

4.2.2 Viability conditions

For a cosmologically viable $f(R)$ model, the following conditions must be satisfied simultaneously:

- (i) *Stability.* The function $f(R)$ must satisfy

$$f_{,R} > 0, \quad f_{,RR} > 0 \quad (4.12)$$

over the entire curvature range of cosmological interest. The first condition ensures that gravitons are not ghosts and that gravity remains attractive; the second prevents the scalar degree of freedom (*scalaron*) from becoming tachyonic in the high-curvature regime.

- (ii) *Newtonian limit.* In the limit $R \gg R_0$, where R_0 denotes the present-day curvature scalar, the model must reduce to GR with small corrections:

$$|f(R) - R| \ll R, \quad |f_{,R} - 1| \ll 1, \quad Rf_{,RR} \ll 1. \quad (4.13)$$

This ensures consistency with the observed small-scale matter inhomogeneities and compact object phenomenology that are well-described by Newtonian gravity.

- (iii) *Solar System and laboratory constraints.* The model must be indistinguishable from GR at the precision of current laboratory experiments and Solar System tests of gravity.

- (iv) *High-curvature GR recovery.* In the high-curvature limit, the model must approach GR with a cosmological constant:

$$\lim_{R \gg R_0} f(R) = R - 2\Lambda, \quad (4.14)$$

which implies $f_{,R}(\infty) = 1$ and therefore $0 < f_{,R}(R) < 1$ for all finite R . This condition also guarantees consistency with CMB observations and the standard thermal history of the Universe, including Big Bang nucleosynthesis and the matter-dominated epoch.

- (v) *Late-time de Sitter attractor.* The model must admit a stable or metastable de Sitter fixed point to account for the observed current phase of accelerated expansion.

These conditions ensure that the model is free from theoretical pathologies and observationally consistent across the full range of cosmologically relevant scales. In particular, they guarantee the recovery of GR in high-curvature regimes, the stability of cosmological solutions, and a viable late-time accelerated phase. Together, they define the physically admissible parameter space of $f(R)$ models.

4.2.3 Starobinsky regularization

A generic issue in viable $f(R)$ models is the emergence of a weak curvature singularity when $f_{,RR} \rightarrow 0$ at finite R , marginally violating the stability condition $f_{,RR} > 0$. In this regime, the scalaron mass $m_\phi^2 \sim 1/(3f_{,RR})$ diverges, leading to pathological behavior such as large-amplitude curvature oscillations in high-curvature environments ($R \gg R_{\text{vac}}$). This problem can be solved by adding a quadratic correction proportional to R^2 , which guarantees $f_{,RR} > 0$ at all curvatures while remaining subdominant at late times. We therefore implement the regularization [11, 48]

$$f(R) \rightarrow f(R) + \frac{R^2}{6M^2}, \quad M^2 \equiv \frac{\epsilon_{f(R)}}{\delta_s}, \quad (4.15)$$

where $\epsilon_{f(R)}$ is the characteristic curvature scale of the model at the present epoch, $\delta_s \ll 1$ is a dimensionless parameter and M characterizes a mass scale coinciding with the scalaron rest-mass whenever low curvature modifications to GR can be neglected. To reproduce the observed amplitude of the primordial power spectrum, one typically requires $M \approx 1.5 \times 10^{-5} (50/N) M_{\text{Pl}}$ at the end of inflation [49].

4.2.4 Appleby-Battye

The Appleby–Battye (AB) model, originally proposed in [9], is defined as

$$f(R) = \frac{R}{2} - \frac{\epsilon_{\text{AB}}}{2} \ln \left[\frac{\cosh\left(\frac{R}{\epsilon_{\text{AB}}} - b\right)}{\cosh(b)} \right], \quad (4.16)$$

where b is a dimensionless parameter controlling the deviation from Λ CDM, and ϵ_{AB} sets the characteristic curvature scale. The latter is fixed by the de Sitter vacuum condition $f(R_{\text{vac}}) = R_{\text{vac}}$:

$$\epsilon_{\text{AB}} = \frac{R_{\text{vac}}}{b + \ln(2 \cosh b)}, \quad (4.17)$$

with $R_{\text{vac}} = 12H_0^2$. The stability condition $b > 1.6$ must be satisfied in order for the model to admit a viable late-time de Sitter solution and reproduce the observed accelerated expansion of the Universe [49–52]. In the limit $b \rightarrow \infty$, as well as for high curvatures $R \gg R_{\text{vac}}$, the model approaches Λ CDM.

4.2.5 Hu-Sawicki

Originally proposed in [10], the Hu-Sawicki (HS) model can be written as¹:

$$f(R) = R - 2\Lambda \frac{R^n}{R^n + \mu_{\text{HS}}^{2n}}, \quad (4.18)$$

where $\Lambda = 3H_0^2(1 - \Omega_m)$ is the effective cosmological constant and n is a positive integer. For $R \gg \mu_{\text{HS}}^2$, the model approaches Λ CDM, and it is exactly recovered in the limit $\mu_{\text{HS}} = 0$. In contrast, for $\mu_{\text{HS}} \rightarrow \infty$ the model reduces to $f(R) = R$, corresponding to GR without a cosmological constant and therefore to a non-accelerating universe.

4.2.6 Starobinsky

Proposed in [11] as a geometric dark energy model, the Starobinsky (ST) model is defined by:

$$f_S(R) = R + \lambda_S R_S \left[\left(1 + \frac{R^2}{R_S^2} \right)^{-n} - 1 \right], \quad (4.19)$$

where $\lambda_S > 0$ and $R_S \sim R_0$ sets the characteristic curvature scale. As in the HS model, n is a positive integer. In the high-curvature regime $R \gg R_S$, the model approaches Λ CDM with an effective cosmological constant $\Lambda = \lambda_S R_S/2$. Imposing consistency with the background expansion today yields

$$R_S = \frac{6H_0^2(1 - \Omega_m)}{\lambda_S}. \quad (4.20)$$

Furthermore, the requirement of a stable late-time de Sitter solution imposes a lower bound on λ_S that depends on n . For representative values, one finds $(n, \lambda_{S,\text{min}}) \simeq (1, 1.54)$, $(2, 0.94)$, $(3, 0.73)$, and $(4, 0.61)$ [53]. Consequently, only a restricted region of the parameter space (λ_S, n) corresponds to physically viable cosmological solutions.

5 Observational Datasets

We constrain the free parameters of all models described in Sec. 4 using four independent late-time datasets composed of 35 $H(z)$ measurements from CC, 1590 light curves from the Pantheon+ SNe Ia compilation (after a $z > 0.01$ redshift cut), 13 BAO measurements from DESI DR2, and 104 FRBs with measured redshifts. All distance observables entering the likelihoods are defined in Sec. 2.2.

Cosmic Chronometers

A well-established approach for probing the expansion history of the Universe in a model-independent way is the Cosmic Chronometers method. This technique relies on the relation $H(z) = -\frac{1}{1+z} \frac{dz}{dt} \approx -\frac{1}{1+z} \frac{\Delta z}{\Delta t}$. The measurement of the CC dataset is inferred from pairs of passively evolving galaxies with old stellar populations, negligible star formation, and slightly different redshifts [54].

In Table 11 we list 35 measurements of $H(z)$, which carry systematic uncertainties mainly associated with stellar population synthesis model (SPS) modeling and potential contamination from residual young stellar populations in the galaxies [55, 56].

¹The original form of the HS model is $f(R) = R - m^2 \frac{c_1(R/m^2)^n}{c_2(R/m^2)^n + 1}$, where $m^2 \equiv \frac{\kappa^2 \rho_0}{3} = H_0^2 \Omega_m$. The parametrization in Eq. (4.18) is obtained by defining $\mu_{\text{HS}}^2 \equiv m^2 c_2^{-1/n}$ and identifying $\Lambda = \frac{m^2 c_1}{2c_2}$.

Type Ia Supernovae

We use the Pantheon+ compilation [57], comprising 1701 light curves of 1550 spectroscopically confirmed SNe Ia over $0.001 \leq z \leq 2.26$, with a full statistical and systematic covariance matrix C_{SNe} . We apply a low-redshift cut $z > 0.01$ to minimize contamination from peculiar velocities, which at very low redshifts become comparable to the Hubble flow and introduce systematic biases in the inferred luminosity distances [58]. The nuisance parameter M_B is treated as a free parameter and constrained jointly with the cosmological parameters, with the uniform prior listed in Table 1.

Baryon Acoustic Oscillations

BAO provides one of the most robust standard rulers in cosmology, enabling precise measurements of the expansion history of the Universe. This characteristic comoving scale originates from sound waves propagating in the photon–baryon plasma before recombination, and is set by the sound horizon at the drag epoch, r_d .

Here, we use 13 BAO measurements from DESI DR2 [59], which includes over 14 million galaxies and quasars spanning the redshift range $0.1 < z < 4.2$. The dataset comprises multiple tracers, including Bright Galaxy Samples (BGS), Luminous Red Galaxies (LRGs), Emission Line Galaxies (ELGs), quasars (QSOs), and Ly α forest measurements, probing a wide range of cosmic epochs. All observables are expressed in units of the sound horizon at the drag epoch, r_d , including measurements of $D_M(z)/r_d$, $D_H(z)/r_d$, and $D_V(z)/r_d$, with r_d calculated according to Eq. (2.8).

Fast Radio Bursts

We use 104 FRBs with spectroscopically confirmed host-galaxy redshifts, compiled from a heterogeneous set of recent surveys and follow-up observations. The sample spans the redshift range $0.0085 \leq z \leq 1.354$, and originates from multiple radio telescope facilities, including CHIME [60], ASKAP/CRAFT [61], and DSA [29, 62, 63], among others [16, 22, 64–70], as shown in Table 12.

The Galactic interstellar contribution $\text{DM}_{\text{MW,ISM}}$ is estimated using the NE2001 electron density model [35], spanning 19.9–188.4 pc cm $^{-3}$ across the sample. The halo contribution $\text{DM}_{\text{MW,halo}}$ remains uncertain, with estimates ranging from ~ 25 –110 pc cm $^{-3}$ depending on the assumed gas distribution and feedback mechanisms [71–74], and potentially direction-dependent in anisotropic models [75]. Following [18, 26, 28], we adopt the fiducial constant value $\text{DM}_{\text{MW,halo}} = 50$ pc cm $^{-3}$, which is representative of current constraints and consistent with the expected baryon fraction of the Milky Way. It is worth stressing that we use both repeating and non-repeating sources in our MCMC routine.

6 Statistical Methodology

We perform a Bayesian inference analysis to constrain the cosmological parameters of each model. According to Bayes’ theorem, the posterior probability distribution is given by

$$P(\boldsymbol{\theta}|D) \propto \mathcal{L}(D|\boldsymbol{\theta}) \pi(\boldsymbol{\theta}), \quad (6.1)$$

where $\boldsymbol{\theta}$ denotes the set of model parameters, D is the observed data, \mathcal{L} is the likelihood function, and $\pi(\boldsymbol{\theta})$ is the prior distribution.

We adopt a combination of uniform (top-hat) priors implemented as hard bounds, together with Gaussian priors for selected parameters, reflecting either minimal assumptions or external constraints from independent observations. Table 1 summarizes the prior distributions adopted for all free parameters.

Parameter	Prior type	Range
H_0 [km s ⁻¹ Mpc ⁻¹]	Uniform	[50, 90]
Ω_m	Uniform	[0.1, 0.6]
Ω_b	Uniform	[0.01, 0.1]
M_B [mag]	Uniform	[-20.0, -18.0]
w	Uniform	[-3, 1]
w_0	Uniform	[-3, 1]
w_a	Uniform	[-3, 2]
b	Uniform	[1.6, 12]
μ_{HS} [km s ⁻¹ Mpc ⁻¹]	Uniform	[0, 300]
λ_S	Uniform	[1.54, 10]
σ_{host}	Uniform	[0.2, 2.0]
e^μ [pc cm ⁻³]	Uniform	[20, 200]

Table 1. Prior distributions adopted for all free parameters. Uniform priors are specified by their bounds $[a, b]$.

For the primary cosmological parameters (H_0 , Ω_m , Ω_b), we assign broad uniform priors so that the constraints are driven entirely by the data; in particular, the range adopted for Ω_b is physically motivated and broad enough to allow it to be constrained directly by the BAO and FRB data, which are sensitive to the baryon density through the sound horizon and the IGM dispersion measure, respectively. For the SNe Ia absolute magnitude M_B , we assign a broad uniform prior, allowing it to be constrained jointly with all the cosmological parameters. Finally, for the extended-model parameters (w , w_0 , w_a , b , μ_{HS} , λ_S) and the FRB nuisance parameters (e^μ , σ_{host}), we adopt uniform priors that are minimally informative and comfortably cover the regions of interest suggested by previous studies and exploratory runs.

6.1 Numerical Implementation

For the GR-based cosmological models (Λ CDM, w CDM, CPL), the Hubble parameter $H(z)$ is computed analytically at each likelihood evaluation. In contrast, the background evolution in $f(R)$ gravity is governed by higher-order differential systems compared to GR. Depending on the structure of each model, the modified Friedmann equations can be recast into equivalent dynamical systems for the background expansion, which are then integrated numerically (see Appendix A for details).

The numerical integration strategy is adapted to the specific structure of each model. For the AB case, whose background evolution is expressed as a third-order ordinary differential equation (ODE) for $H(a)$ and remains numerically well behaved over the relevant redshift range, we use the explicit high-order Runge–Kutta solver DOP853, which is well suited for smooth, non-stiff systems. In contrast, for the HS and ST models, which are formulated as second-order systems in the variable $y_H(\ln a)$ and can exhibit stiffness due to the scalaron

dynamics at low curvature, we employ the LSODA solver [76], which automatically switches between stiff and non-stiff integration schemes.

Since repeated ODE integrations during the MCMC sampling would be computationally prohibitive, we adopt a two-step strategy. First, the background equations are solved over a precomputed grid in $(H_0, \Omega_m, \theta_{f(R)}, z)$, covering the redshift range $z \in [0, 4]$. Second, during sampling, $H(z)$ is evaluated via interpolation over this grid, reducing each likelihood call to an inexpensive lookup. Full details of the grid construction and validation are given in Appendix C.

6.2 Joint Likelihood

Assuming statistical independence between the different datasets (while fully accounting for internal covariances within each dataset), the total log-likelihood is constructed as the sum of the individual contributions:

$$\ln \mathcal{L}_{\text{tot}} = \ln \mathcal{L}_{\text{CC}} + \ln \mathcal{L}_{\text{SNe}} + \ln \mathcal{L}_{\text{BAO}} + \ln \mathcal{L}_{\text{FRB}}. \quad (6.2)$$

The CC likelihood is adopted as a Gaussian:

$$\ln \mathcal{L}_{\text{CC}} = -\frac{1}{2} \sum_i \left[\frac{H_{\text{obs}}(z_i) - H_{\text{th}}(z_i)}{\sigma_{H,i}} \right]^2, \quad (6.3)$$

where $H_{\text{obs}}(z_i)$ and $\sigma_{H,i}$ are the observed Hubble parameter and its uncertainty at redshift z_i , and $H_{\text{th}}(z_i)$ is the model prediction.

The SNe likelihood accounts for the full inter-supernova covariance:

$$\ln \mathcal{L}_{\text{SNe}} = -\frac{1}{2} \Delta \mathbf{m}_B^T C_{\text{SNe}}^{-1} \Delta \mathbf{m}_B, \quad (6.4)$$

where $\Delta \mathbf{m}_B = \mathbf{m}_{B,\text{obs}} - \mathbf{m}_{B,\text{th}}$ and $\mathbf{m}_{B,\text{th}}$ is evaluated via Eq. (2.6).

The BAO likelihood is analogously constructed using the full covariance matrix:

$$\ln \mathcal{L}_{\text{BAO}} = -\frac{1}{2} \Delta \mathbf{d}^T C_{\text{BAO}}^{-1} \Delta \mathbf{d}, \quad (6.5)$$

where $\Delta \mathbf{d} = \mathbf{d}_{\text{obs}} - \mathbf{d}_{\text{th}}$ and \mathbf{d}_{th} is the model prediction for the BAO observables.

The FRB likelihood is constructed by marginalizing over the unobserved host-galaxy contribution. Given the decomposition of Eq. (3.4), the probability of measuring $\text{DM}_{\text{ext},i}$ at known redshift z_i is obtained by convolving P_{IGM} and P_{host} :

$$\ln \mathcal{L}_{\text{FRB}} = \sum_i \ln P(\text{DM}_{\text{ext},i} | z_i), \quad (6.6)$$

with the marginal probability density function (PDF)

$$P(\text{DM}_{\text{ext}} | z) = \frac{1}{\langle \text{DM}_{\text{IGM}} \rangle} \int_0^{\text{DM}_{\text{ext}}(1+z)} P_{\text{IGM}} \left(\frac{\text{DM}_{\text{ext}} - (1+z)^{-1} \text{DM}_{\text{host}}}{\langle \text{DM}_{\text{IGM}} \rangle} \right) P_{\text{host}}(\text{DM}_{\text{host}}) d\text{DM}_{\text{host}}, \quad (6.7)$$

where P_{IGM} and P_{host} are defined in Eqs. (3.7) and (3.10), and the normalization factor $\langle \text{DM}_{\text{IGM}} \rangle^{-1}$ ensures that the PDF of DM_{ext} integrates to unity [28, 42, 46].

6.3 Figure of Merit

To quantify the impact of FRBs on the cosmological constraints, we evaluate the Figure of Merit (FoM) in the two-dimensional parameter space (H_0, Ω_b) . This choice is physically motivated by the direct sensitivity of FRB dispersion measures to the cosmic baryon content, Ω_b , which provides information complementary to the standard sound-horizon constraints from BAO observations.

Since some of the posterior distributions obtained in this work exhibit mild deviations from Gaussianity, particularly in extended cosmological models, we adopt a non-parametric definition of the FoM based on the highest-posterior-density (HPD) region of the joint posterior distribution. The two-dimensional posterior is reconstructed using a Gaussian kernel density estimator (KDE), and the FoM is defined as

$$\text{FoM}_{\text{HPD}} = \frac{1}{A_{68.3}}, \quad (6.8)$$

where $A_{68.3}$ denotes the area enclosed by the 68.3% HPD contour in the (H_0, Ω_b) plane.

The HPD contour is determined by identifying the density threshold that encloses 68.3% of the total posterior probability. Consequently, the FoM directly measures the constraining power of a given dataset through the inverse area of the corresponding credible region. Smaller credible regions therefore correspond to larger FoM values.

This definition does not assume Gaussian or elliptical posterior distributions and naturally reduces to the standard covariance-based FoM for approximately Gaussian posteriors. As a result, the adopted estimator provides a robust measure of the constraining power even in the presence of asymmetric or mildly non-Gaussian posterior distributions.

For completeness, we additionally report effective marginal uncertainties derived from the 16th and 84th percentiles of the posterior samples, together with the skewness of the one-dimensional distributions. These quantities serve as diagnostics of the posterior shape but do not enter the definition of the FoM itself.

6.4 Model Selection Criteria

To compare models with different numbers of free parameters, we employ information criteria that penalize model complexity, following the principle of parsimony. The AIC and BIC are defined as

$$\text{AIC} = 2k - 2 \ln \mathcal{L}_{\text{max}}, \quad \text{BIC} = k \ln N_{\text{tot}} - 2 \ln \mathcal{L}_{\text{max}}, \quad (6.9)$$

where k is the number of free parameters, N_{tot} is the total number of data points, and \mathcal{L}_{max} is the maximum likelihood. We report differences ΔAIC and ΔBIC relative to ΛCDM , which serves as the baseline model. The interpretation of $\Delta\text{IC} \equiv \Delta\text{AIC}$ or ΔBIC follows [77], where a negative (positive) ΔIC indicates preference for the alternative (reference) model, with strength classified as:

- $|\Delta\text{IC}| \in [0, 2]$: weak evidence, inconclusive;
- $|\Delta\text{IC}| \in (2, 6]$: positive evidence;
- $|\Delta\text{IC}| \in (6, 10]$: strong evidence;
- $|\Delta\text{IC}| > 10$: very strong evidence.

All models considered in this work are extensions of Λ CDM. Therefore, Λ CDM can be recovered as a limiting case for specific values of the additional parameters. For this reason, we additionally apply the likelihood-ratio test (LRT) as a complementary model-comparison criterion. Under the null hypothesis that Λ CDM is the true model, the statistic

$$\Lambda_{\text{LR}} = -2 \ln \frac{\mathcal{L}_{\Lambda\text{CDM}}}{\mathcal{L}_{\text{alt}}} \quad (6.10)$$

follows asymptotically a χ^2 distribution with Δk degrees of freedom [78]. The p -value is then obtained directly from this distribution as

$$p = P\left(\chi_{\Delta k}^2 \geq \Lambda_{\text{LR}}^{\text{obs}}\right) = 1 - F_{\chi_{\Delta k}^2}\left(\Lambda_{\text{LR}}^{\text{obs}}\right), \quad (6.11)$$

where $F_{\chi_{\Delta k}^2}$ is the cumulative distribution function of the χ^2 distribution with Δk degrees of freedom. A value of $p < 0.05$ indicates that the improvement in fit is statistically significant and that the extra parameters are warranted by the data. On the other hand, $p \geq 0.05$ suggests that the additional complexity is not justified relative to Λ CDM model.

7 Results and discussions

The results of the observational constraints for all six cosmological scenarios considered in Sec. 4 are now presented, where we quantify the impact of incorporating FRB observations into standard cosmological probes and evaluate the relative performance of each model using model selection criteria already discussed. For clarity, we define two data combinations used throughout this work: the Baseline dataset, corresponding to CC + SNe + BAO, and the Baseline + FRB dataset, corresponding to CC + SNe + BAO + FRB. Our analysis focuses on precision gains, degeneracy breaking, the constraining power of FRBs, and the statistical comparison among the different cosmological scenarios analyzed.

7.1 Λ CDM

The posterior distributions for the Λ CDM model are shown in Fig. 1, while the corresponding marginalized constraints are summarized in Table 2. The Baseline dataset already provides tight constraints on the expansion history. The inclusion of FRB observations, however, significantly enhances the overall precision. In particular, the uncertainty in the Hubble constant H_0 decreases from ~ 1.53 to ~ 1.04 $\text{km},\text{s}^{-1},\text{Mpc}^{-1}$ (a 31.1% improvement), the uncertainty in the baryon density Ω_b decreases from ~ 0.0025 to ~ 0.0017 (a 30.6% improvement), and the uncertainty in the SNe Ia absolute magnitude M_B decreases from ~ 0.047 to ~ 0.032 (a 31.6% improvement). In contrast, the matter density parameter Ω_m remains essentially unchanged, as it is already tightly constrained by geometric probes and only weakly correlated with the FRB observable.

These improvements are clearly illustrated in Fig. 1, where the inclusion of FRB data significantly alleviates the H_0 - M_B and H_0 - Ω_b degeneracies. This effect is evidenced by the contraction and partial rotation of the posterior contours, indicating that FRBs provide additional information that is largely complementary to the Baseline dataset. Consequently, the allowed parameter volume is substantially reduced, making the Λ CDM model a useful reference case for assessing the impact of FRBs on more extended cosmological scenarios.

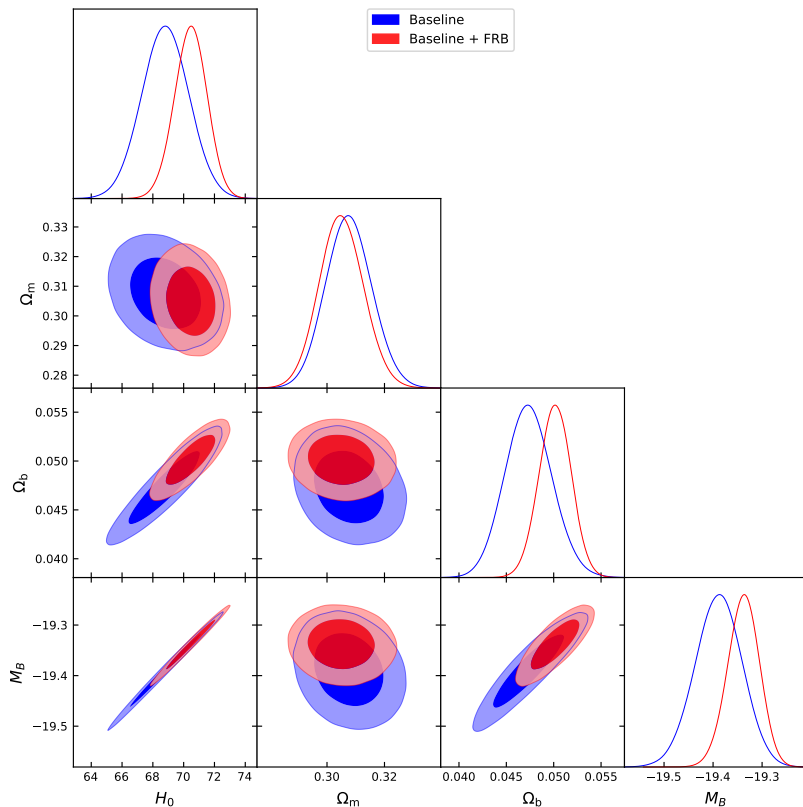


Figure 1. Posterior distributions for the Λ CDM model for the Baseline dataset (blue) and including FRBs (red). Contours correspond to the 68% and 95% credible regions.

Parameter	Baseline	Baseline + FRB
H_0	$68.81^{+1.53}_{-1.52}$	$70.46^{+1.04}_{-1.06}$
Ω_m	0.308 ± 0.008	0.305 ± 0.008
Ω_b	$0.0473^{+0.0025}_{-0.0024}$	0.0501 ± 0.0017
M_B	$-19.388^{+0.047}_{-0.048}$	$-19.338^{+0.032}_{-0.033}$
σ_{host}	—	$0.833^{+0.124}_{-0.102}$
e^μ	—	$104.2^{+16.2}_{-15.8}$

Table 2. Marginalized constraints at 68% confidence level for the Λ CDM model, obtained from the baseline dataset and from the combined dataset including FRBs.

7.2 w CDM

The posterior distributions for the w CDM model are shown in Fig. 2, with the corresponding marginalized constraints listed in Table 3. Allowing for a free dark energy EoS parameter introduces additional freedom in the expansion history, leading to stronger degeneracies between the expansion rate and the dark energy sector. The inclusion of FRBs nevertheless improves the constraints on several cosmological parameters. In particular, the uncertainty in the Hubble constant H_0 decreases from ~ 1.56 to ~ 1.30 $\text{km},\text{s}^{-1},\text{Mpc}^{-1}$ (a 16.4% improvement), while the uncertainty in the baryon density parameter Ω_b decreases from ~ 0.0041 to ~ 0.0026

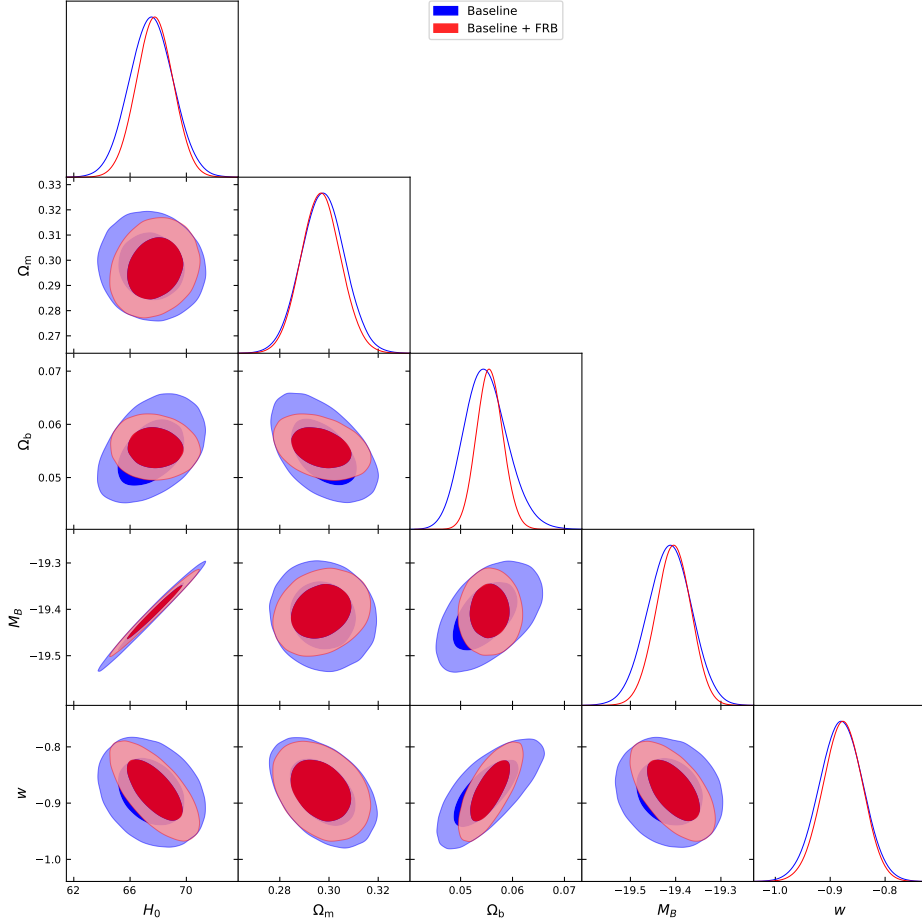


Figure 2. Posterior distributions for the w CDM model for the Baseline dataset (blue) and including FRBs (red). Contours correspond to the 68% and 95% credible regions.

Parameter	Baseline	Baseline + FRB
H_0	$67.51^{+1.56}_{-1.55}$	67.75 ± 1.30
Ω_m	0.298 ± 0.009	0.297 ± 0.008
Ω_b	$0.0548^{+0.0043}_{-0.0039}$	$0.0556^{+0.0026}_{-0.0025}$
M_B	$-19.413^{+0.048}_{-0.049}$	$-19.405^{+0.038}_{-0.039}$
w	$-0.880^{+0.039}_{-0.040}$	-0.877 ± 0.036
σ_{host}	—	$0.860^{+0.134}_{-0.111}$
e^μ	—	$95.0^{+16.3}_{-15.8}$

Table 3. Marginalized constraints at 68% confidence level for the w CDM model, obtained from the baseline dataset and from the combined dataset including FRBs.

(a 37.8% improvement). The uncertainty in the SNe Ia absolute magnitude M_B is also reduced from ~ 0.049 to ~ 0.039 (a 20.6% improvement). In contrast, the dark energy parameter w exhibits only a modest reduction in its uncertainty, from ~ 0.040 to ~ 0.036 (an 8.9% improvement).

This behavior is illustrated in Fig. 2, where the inclusion of FRBs leads to a visible contraction of the posterior contours, particularly along directions involving Ω_b . However, the degeneracies associated with the dark-energy parameter persist, limiting the propagation of the FRB information to the expansion history. As a result, the additional freedom introduced by w partially absorbs the constraining power of the FRB data, reducing their impact on the dark-energy sector compared to the standard Λ CDM model.

7.3 CPL

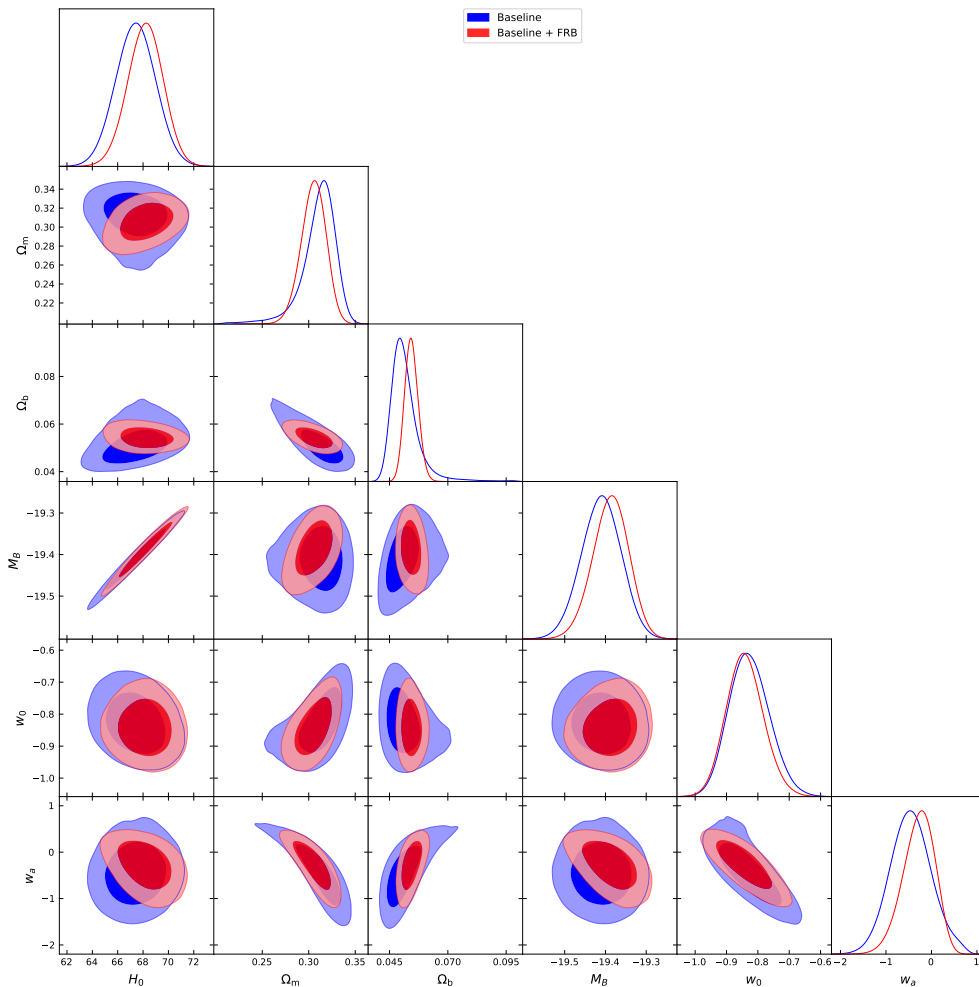


Figure 3. Posterior distributions for the CPL model for the Baseline dataset (blue) and including FRBs (red). Contours correspond to the 68% and 95% credible regions.

The posterior distributions for the CPL model are shown in Fig. 3, with the corresponding marginalized constraints reported in Table 4. The inclusion of FRB data improves the constraints on several cosmological parameters, although the gains are generally smaller than those obtained in the simpler Λ CDM and w CDM scenarios. The largest improvement is observed in the baryon density Ω_b , whose uncertainty reduced from ~ 0.0051 to ~ 0.0029 (a 43.1% improvement). On the other hand, the uncertainty in H_0 decreased from ~ 1.56 to $\sim 1.38 \text{ km s}^{-1} \text{ Mpc}^{-1}$ (a 11.5% improvement), and the uncertainty in M_B decreased

Parameter	Baseline	Baseline + FRB
H_0	67.42 ± 1.56	$68.20^{+1.36}_{-1.40}$
Ω_m	$0.313^{+0.014}_{-0.018}$	$0.306^{+0.013}_{-0.014}$
Ω_b	$0.0506^{+0.0059}_{-0.0042}$	$0.0543^{+0.0030}_{-0.0028}$
M_B	$-19.410^{+0.048}_{-0.049}$	$-19.386^{+0.043}_{-0.045}$
w_0	$-0.829^{+0.067}_{-0.061}$	$-0.842^{+0.060}_{-0.057}$
w_a	$-0.457^{+0.457}_{-0.442}$	$-0.261^{+0.327}_{-0.371}$
σ_{host}	—	$0.851^{+0.132}_{-0.108}$
e^μ	—	$98.6^{+17.0}_{-16.7}$

Table 4. Marginalized constraints at 68% confidence level for the CPL model, obtained from the baseline dataset and from the combined dataset including FRBs.

from ~ 0.049 to ~ 0.044 (a 10.2% improvement). The dark energy sector, in turn, shows limited improvement in w_0 , with the uncertainty decreasing from ~ 0.064 to ~ 0.059 (a 7.8% improvement), while w_a exhibits a moderate improvement, with its uncertainty decreasing from ~ 0.45 to ~ 0.35 (a 22.2% improvement).

The reduced impact of FRBs in the CPL model originates from the enlarged parameter space introduced by the (w_0, w_a) sector. Strong correlations involving H_0 , w_0 , and w_a absorb part of the constraining power provided by the FRB data, limiting the propagation of the baryon-density information to the expansion history. This behavior is clearly illustrated in Fig. 3, where the posterior contours exhibit a visible contraction, particularly along directions associated with Ω_b , while the extended degeneracies in the (w_0, w_a) plane persist. Consequently, although FRBs substantially improve the determination of the baryon content, their ability to constrain the dark-energy sector remains limited in the CPL parametrization.

7.4 Appleby-Battye

The posterior distributions for the AB model are shown in Fig. 4, with the corresponding marginalized constraints reported in Table 5. The inclusion of FRB data leads to substantial improvements in the cosmological parameter constraints, closely resembling the behavior observed in the Λ CDM scenario. In particular, the uncertainty in the Hubble constant H_0 decreases from ~ 1.59 to $\sim 1.08 \text{ km, s}^{-1}, \text{ Mpc}^{-1}$ (a 31.9% improvement), while the uncertainty in the baryon density Ω_b decreases from ~ 0.0025 to ~ 0.0017 (a 32.0% improvement). The uncertainty in the SNe Ia absolute magnitude M_B also decreases from ~ 0.049 to ~ 0.033 (a 33.0% improvement).

This behavior is illustrated in Fig. 4, where the inclusion of FRB data produces a noticeable contraction and partial rotation of the posterior contours, particularly in the H_0 – Ω_b and H_0 – M_B planes. The similarity between the AB and Λ CDM results reflects the fact that the AB expansion history rapidly approaches the standard cosmological model over a wide region of parameter space.

The additional parameter b remains only weakly constrained, with the lower bound shifting slightly from $b > 6.123$ to $b > 6.319$ after the inclusion of FRBs. As b increases, the AB model rapidly approaches the Λ CDM limit, becoming effectively indistinguishable from it at the level of current observations. Consequently, the likelihood becomes increasingly flat for $b \gtrsim 6$, leading to a posterior dominated by prior volume at large values of b . As a result, neither a meaningful upper bound nor a well-defined central value can be determined,

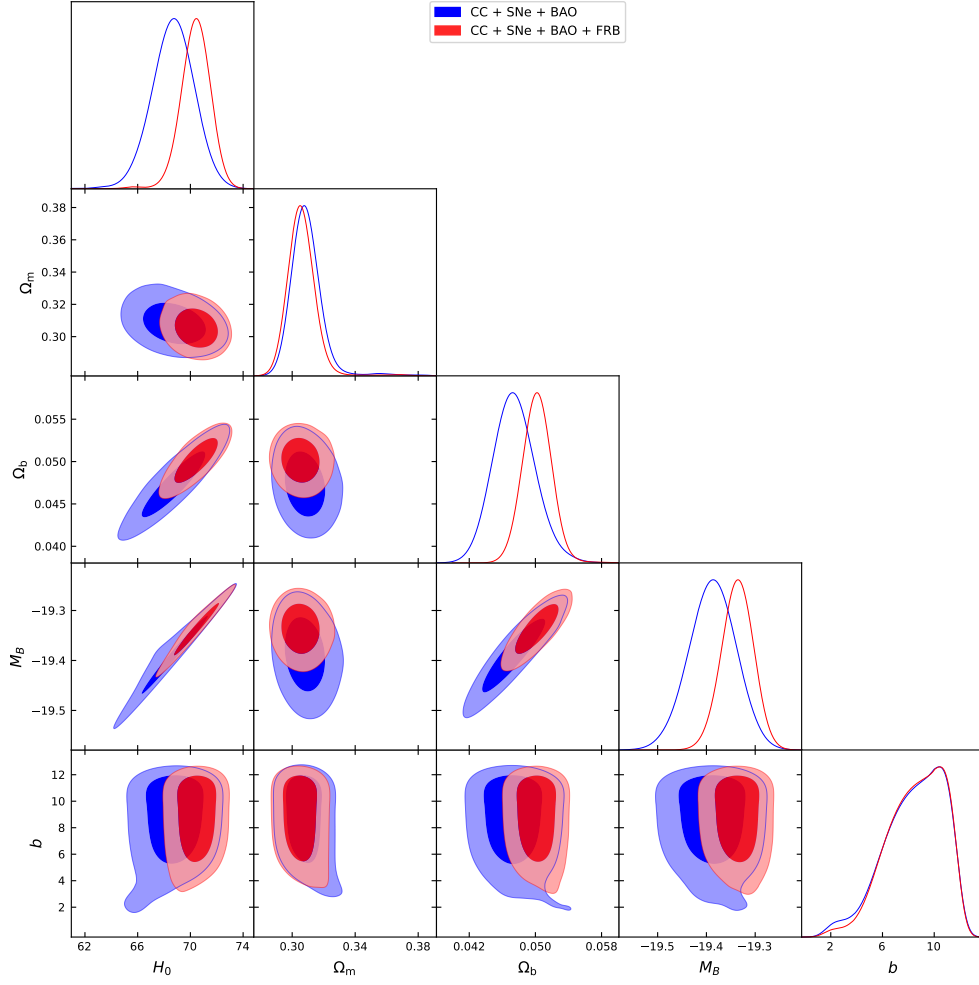


Figure 4. Posterior distributions for the AB model for the Baseline dataset (blue) and including FRBs (red). Contours correspond to the 68% and 95% credible regions.

Parameter	Baseline	Baseline + FRB
H_0	$68.71^{+1.56}_{-1.61}$	$70.42^{+1.06}_{-1.10}$
Ω_m	$0.308^{+0.009}_{-0.008}$	0.305 ± 0.008
Ω_b	$0.0474^{+0.0026}_{-0.0024}$	0.0502 ± 0.0017
M_B	$-19.387^{+0.048}_{-0.049}$	$-19.336^{+0.032}_{-0.033}$
b	> 6.123	> 6.319
σ_{host}	—	$0.834^{+0.123}_{-0.102}$
e^μ	—	$104.3^{+16.1}_{-15.2}$

Table 5. Marginalized constraints at 68% confidence level for the AB model, obtained from the baseline dataset and from the combined dataset including FRBs.

indicating that current late-time observations remain largely insensitive to deviations from Λ CDM within this class of models.

7.5 Hu-Sawicki

The posterior distributions for the HS model ($n = 1$) are shown in Fig. 5, with the corresponding marginalized constraints reported in Table 6. The inclusion of FRB data leads to substantial improvements in the cosmological parameter constraints, comparable to, or slightly stronger than, those obtained in the AB model. In particular, the uncertainty in the Hubble constant H_0 decreases from ~ 1.60 to ~ 1.04 $\text{km},\text{s}^{-1},\text{Mpc}^{-1}$ (a 34.8% improvement), while the uncertainty in the baryon density Ω_b decreases from ~ 0.0029 to ~ 0.0017 (a 40.4% improvement). The uncertainty in the SNe Ia absolute magnitude M_B also decreases from ~ 0.049 to ~ 0.036 (a 25.8% improvement).

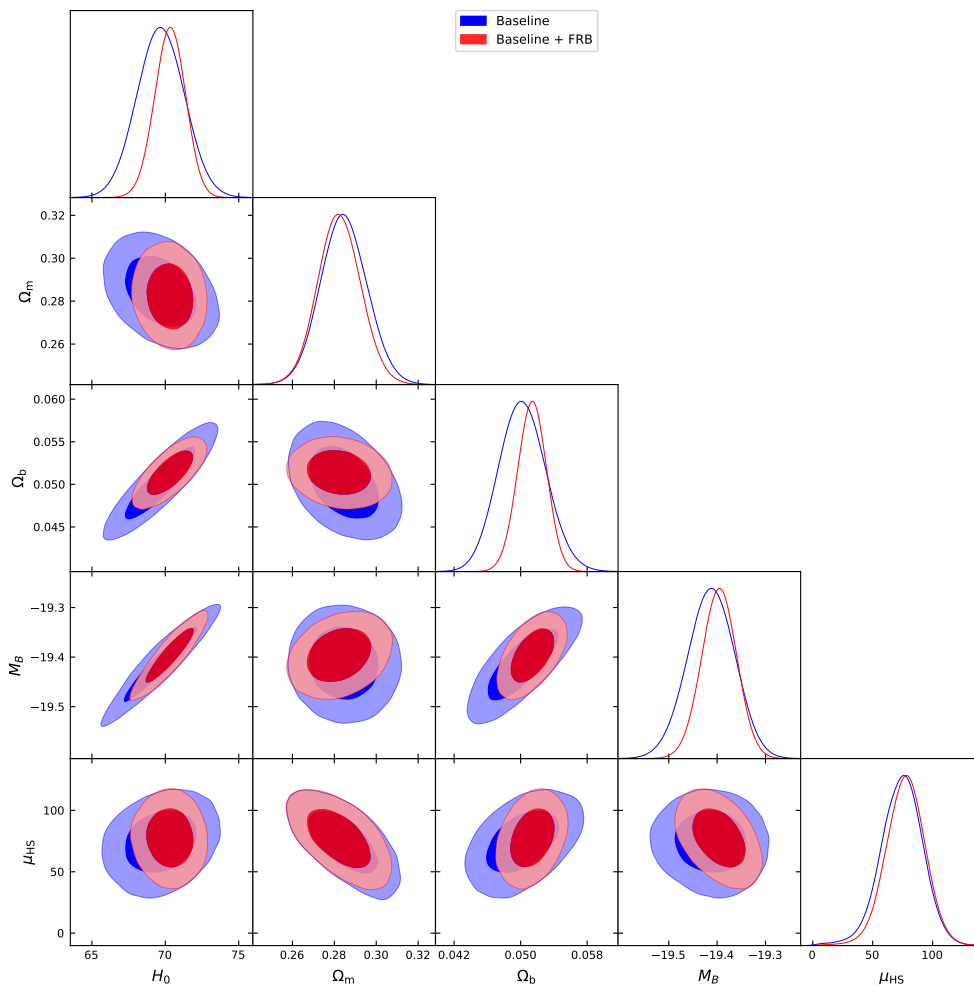


Figure 5. Posterior distributions for the HS model for the Baseline dataset (blue) and including FRBs (red). Contours correspond to the 68% and 95% credible regions.

As illustrated in Fig. 5, the inclusion of FRB data produces a visible contraction and mild rotation of the posterior contours, particularly in the H_0 - Ω_b and H_0 - M_B planes. The overall behavior closely resembles that observed in the AB model, indicating that FRBs efficiently constrain the background cosmological parameters while the modified-gravity sector remains comparatively less affected.

Parameter	Baseline	Baseline + FRB
H_0	$69.69^{+1.60}_{-1.59}$	$70.32^{+1.03}_{-1.05}$
Ω_m	0.284 ± 0.011	0.282 ± 0.010
Ω_b	$0.0502^{+0.0029}_{-0.0028}$	0.0514 ± 0.0017
M_B	$-19.412^{+0.048}_{-0.049}$	-19.396 ± 0.036
μ_{HS}	$74.59^{+16.55}_{-17.45}$	$77.54^{+15.68}_{-16.24}$
σ_{host}	—	$0.857^{+0.132}_{-0.109}$
e^μ	—	$96.7^{+16.4}_{-15.9}$

Table 6. Marginalized constraints at 68% confidence level for the HS model, obtained from the baseline dataset and from the combined dataset including FRBs.

The modified gravity parameter μ_{HS} remains only weakly constrained, with a broad posterior distribution and no significant reduction in its uncertainty after the inclusion of FRBs. Although the posterior peaks at a non-zero value, corresponding to an approximately 4.7σ offset from the GR limit $\mu_{\text{HS}} = 0$, this should not be interpreted as evidence for deviations from Λ CDM. Instead, it reflects the bounded and non-Gaussian nature of the posterior distribution, together with volume effects in parameter space. As shown in Fig. 5, μ_{HS} exhibits moderate correlations with H_0 , Ω_m , and Ω_b , but these correlations are insufficient to significantly tighten its constraint. Unlike the AB model, however, the posterior retains a well-defined peak and is not dominated by prior volume, indicating that current late-time observations still provide limited, but non-negligible, sensitivity to this parameter.

7.5.1 Starobinsky

The posterior distributions for the ST model are shown in Fig. 6, with the corresponding marginalized constraints reported in Table 7. The inclusion of FRB data improves the cosmological parameter constraints, although the gains are generally smaller than those obtained in the AB and HS models. In particular, the uncertainty in the Hubble constant H_0 decreases from ~ 1.67 to ~ 1.30 $\text{km,s}^{-1},\text{Mpc}^{-1}$ (a 21.9% improvement), while the uncertainty in the baryon density Ω_b decreases from ~ 0.0030 to ~ 0.0022 (a 25.4% improvement). A larger gain is observed for the SNe Ia absolute magnitude M_B , whose uncertainty decreases from ~ 0.048 to ~ 0.033 (a 31.6% improvement).

As illustrated in Fig. 6, the inclusion of FRB data produces a visible contraction and mild rotation of the posterior contours, particularly in the H_0 – M_B plane. The comparatively larger improvement observed for M_B reflects the partial alleviation of its degeneracy with the Hubble constant, whereas the impact on the remaining cosmological parameters is more moderate than in the AB and HS scenarios.

The modified-gravity parameter λ_S remains only weakly constrained, exhibiting a broad and asymmetric posterior distribution with no significant reduction in its uncertainty after the inclusion of FRBs. Nevertheless, the posterior displays a well-defined peak around $\lambda_S \sim 2$ and does not extend toward arbitrarily large values, indicating that the likelihood does not become fully flat in the Λ CDM limit. This behavior suggests that, unlike the AB model, current observations retain some sensitivity to the modified-gravity sector, although the overall constraining power remains limited.

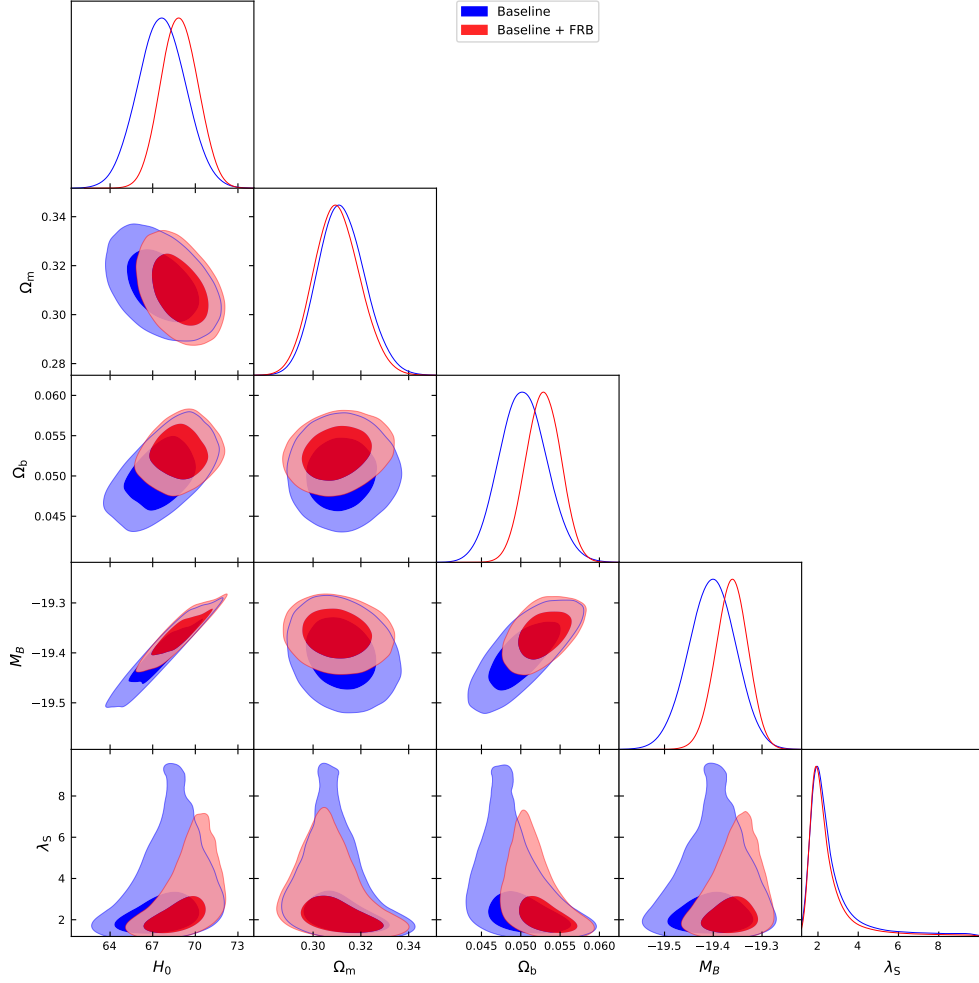


Figure 6. Posterior distributions for the ST model for the baseline dataset (blue) and including FRBs (red). Contours correspond to the 68% and 95% credible regions.

Parameter	CC + SNe + BAO	CC + SNe + BAO + FRB
H_0	$67.64^{+1.67}_{-1.66}$	$68.87^{+1.32}_{-1.28}$
Ω_m	$0.312^{+0.010}_{-0.009}$	$0.310^{+0.010}_{-0.009}$
Ω_b	$0.0503^{+0.0030}_{-0.0029}$	0.0529 ± 0.0022
M_B	$-19.402^{+0.047}_{-0.048}$	$-19.362^{+0.032}_{-0.033}$
λ_S	$2.17^{+1.29}_{-0.47}$	$2.10^{+1.08}_{-0.42}$
σ_{host}	—	$0.842^{+0.127}_{-0.105}$
e^μ	—	$101.2^{+16.1}_{-15.7}$

Table 7. Marginalized constraints at 68% confidence level for the ST model, obtained from the baseline dataset and from the combined dataset including FRBs.

7.6 FRB nuisance parameters

The posterior distributions for the FRB nuisance parameters, σ_{host} and e^μ , exhibit reasonable stability across the diverse set of cosmological scenarios explored in this work, as evidenced by the marginalized constraints reported in Tables 2–7. For the intrinsic host scatter, we find consistent constraints within the interval $\sigma_{\text{host}} \in [0.833, 0.860]$, with relative 1σ uncertainties ranging from approximately 12% to 16%. Similarly, the log-normal normalization parameter e^μ remains well constrained within the range 95.0–104.3, exhibiting relative 1σ uncertainties of about 15%–17% across all gravitational frameworks.

We further emphasize that even in the presence of additional degrees of freedom, such as the models analyzed here, the posterior distributions for the nuisance sector do not exhibit significant broadening or signs of prior dominance. The stability of the relative uncertainties suggests that the current FRB dataset possesses sufficient sensitivity to mitigate potential degeneracies between astrophysical host contributions and the underlying cosmological signal. Consequently, the robustness of these constraints across both GR-based and modified gravity frameworks provides strong evidence for the internal consistency of the FRB likelihood.

7.7 The Impact of FRBs

We quantify the additional constraining power provided by FRB observations by evaluating both FoM and the 68.3% credible-region area $A_{68.3}$ in the (H_0, Ω_b) plane, following the methodology described in Sec. 6.3. The complementarity between the Baseline dataset and FRBs is particularly important because, while the BAO scale depends on the baryon density through the sound horizon at the drag epoch r_d , the dispersion measures of FRBs provide an independent late-time probe of the cosmic baryon content. This additional information helps to break the degeneracy between the expansion rate and the baryon density.

As summarized in Table 8, the inclusion of FRB data systematically reduces the area of the joint confidence regions and consequently increases the FoM for all cosmological scenarios considered. The reduction in $A_{68.3}$ ranges from approximately 33% in the Λ CDM model to nearly 48% in the CPL parametrization, indicating a substantial contraction of the allowed parameter space. Correspondingly, the FoM increases by 48.4% in the standard Λ CDM scenario and reaches a maximum improvement of 90.8% for the CPL model.

Model	$A_{68.3}$		FoM		Improvement
	Baseline	+FRB	Baseline	+FRB	
Λ CDM	0.0120	0.0081	83.6	124.0	48.4%
w CDM	0.0455	0.0249	22.0	40.2	82.6%
CPL	0.0564	0.0296	17.7	33.8	90.8%
AB	0.0139	0.0090	71.7	111.2	55.1%
HS	0.0157	0.0098	63.5	102.2	61.0%
ST	0.0336	0.0215	29.8	46.6	56.4%

Table 8. Comparison of the 68.3% credible-region area and the Figure of Merit in the (H_0, Ω_b) plane before and after the inclusion of FRB data. The last column gives the relative improvement in the FoM due to the FRB contribution.

The largest gains are observed in the dynamical dark-energy scenarios, particularly CPL and w CDM, where parameter degeneracies are intrinsically stronger. In these cases, FRBs provide an additional constraint direction that efficiently reduces the volume of the

Model	$\sigma(H_0)$		$\sigma(\Omega_b)$		Skew(H_0)		Skew(Ω_b)	
	Baseline	+FRB	Baseline	+FRB	Baseline	+FRB	Baseline	+FRB
Λ CDM	1.524	1.048	0.00246	0.00168	0.000	-0.074	0.121	-0.043
w CDM	1.557	1.298	0.00415	0.00253	0.023	-0.009	0.314	0.089
CPL	1.563	1.384	0.00504	0.00288	0.019	-0.077	2.391	0.197
AB	1.584	1.079	0.00253	0.00173	-0.226	-0.601	0.251	0.286
HS	1.600	1.037	0.00281	0.00171	0.022	-0.065	0.120	-0.046
ST	1.667	1.301	0.00299	0.00221	0.023	0.037	0.121	-0.023

Table 9. Marginal uncertainties and skewness coefficients of the one-dimensional posterior distributions for H_0 and Ω_b before and after the inclusion of FRB data.

posterior distribution. Similarly, the modified-gravity models AB, HS, and ST also exhibit significant improvements, with FoM increases ranging from approximately 55% to 61%. These results further demonstrate the enhanced constraining power of FRBs in extended cosmological scenarios, where additional degrees of freedom typically introduce stronger parameter degeneracies.

The impact of FRBs on the one-dimensional posterior distributions is summarized in Table 9. The inclusion of FRB observations systematically reduces the marginal uncertainties of both H_0 and Ω_b , leading to more precise parameter estimates across all cosmological models. In addition, the skewness coefficients reveal that FRB data generally produce more symmetric posterior distributions. This effect is particularly evident for the CPL model, where the skewness of the Ω_b posterior decreases dramatically from 2.391 to 0.197, indicating a substantial reduction in non-Gaussian features. Similar, although less pronounced, changes are observed in the remaining models. Overall, FRBs not only tighten the cosmological constraints but also regularize the posterior distributions, yielding likelihood surfaces that are closer to Gaussian and consequently more robust for parameter inference.

7.8 Model Comparison

To evaluate the statistical performance of the models considered in this work, we employ the AIC, BIC, and LRT p -value, following the methodology outlined in Sec. 6.4. Table 10 summarizes the statistical performance of each cosmological framework against the full Baseline + FRB dataset, using Λ CDM as reference.

All extended cosmological scenarios considered in this work, except the AB model, provide an improved fit relative to Λ CDM. In particular, the w CDM, CPL, HS, and ST frameworks reduce the best-fit χ^2 by $|\Delta\chi^2| \approx 10$, corresponding to a modest decrease in χ^2/dof from 1.596 to ~ 1.591 . In contrast, the AB model yields a slightly worse fit, with $\Delta\chi^2 = +0.26$.

According to the AIC, the w CDM, CPL, HS, and ST models are strongly favored over Λ CDM, with $\Delta\text{AIC} < -7$, indicating that the improvement in fit outweighs the penalty associated with the additional degrees of freedom. The AB model is instead mildly disfavored ($\Delta\text{AIC} > +2$) relative to the standard model.

When adopting the more conservative BIC, which imposes a stronger penalty on model complexity ($k \ln N \approx 7.46, k$), only w CDM, HS, and ST retain positive evidence relative to Λ CDM, with $-3.2 < \Delta\text{BIC} < -2.7$. The CPL parametrization is penalized due to its larger parameter space ($\Delta\text{BIC} \simeq +3.9$), while the AB model is strongly disfavored ($\Delta\text{BIC} \simeq +7.7$).

The LRT further quantifies the statistical improvement achieved by nested extensions of the Λ CDM model. The w CDM, CPL, HS, and ST models yield p -values ranging from 0.0011

Quantity	Λ CDM	w CDM	CPL	AB	HS	ST
k	6	7	8	7	7	7
$\ln \mathcal{L}_{\max}$	-1383.3235	-1378.0069	-1377.7934	-1383.4515	-1378.2402	-1378.2307
χ^2	2766.6470	2756.0138	2755.5868	2766.9030	2756.4804	2756.4614
χ^2/dof	1.5955	1.5903	1.5910	1.5966	1.5906	1.5906
AIC	2778.6470	2770.0137	2771.5868	2780.9029	2770.4804	2770.4615
BIC	2811.4168	2808.2452	2815.2799	2819.1344	2808.7119	2808.6930
Δ AIC	0	-8.6333	-7.0602	+2.2559	-8.1666	-8.1855
Δ BIC	0	-3.1716	+3.8631	+7.7176	-2.7049	-2.7238
AIC verdict	Ref.	Str. alt.	Str. alt.	Pos. ref.	Str. alt.	Str. alt.
BIC verdict	Ref.	Pos. alt.	Pos. ref.	Str. ref.	Pos. alt.	Pos. alt.
LRT p -value	—	0.0011	0.0040	1.0000	0.0014	0.0014

Table 10. Model comparison statistics for the full CC + SNe + BAO + FRB data combination, using Λ CDM as the reference model. The abbreviations mean Pos. alt. (positive evidence for the alternative model); Pos. ref. (positive evidence for the reference model); Str. alt. (strong evidence for the alternative model); and Str. ref. (strong evidence for the reference model).

to 0.0040, indicating a statistically significant improvement over Λ CDM at the $\alpha = 0.05$ level, corresponding to an approximate 3σ preference for these extensions. In contrast, the AB model yields $p = 1.000$, indicating no statistical preference relative to Λ CDM.

Overall, the results point to a moderate statistical preference for extensions beyond Λ CDM, although the evidence remains inconclusive. While several models yield improved fits to the data, the corresponding BIC differences are limited to $|\Delta\text{BIC}| < 3.2$, placing them within the weak-to-positive evidence regime. This indicates that the observed gains in goodness of fit are not sufficient to decisively favor more complex models once the penalty for additional parameters is taken into account. These findings underscore the sensitivity of model selection to the trade-off between goodness of fit and model complexity, as well as to the choice of statistical criterion.

8 Conclusion

In this work, we have performed a comprehensive cosmological analysis combining CC, SNe Ia, BAO, and FRB datasets to constrain six cosmological scenarios: the standard Λ CDM model, two dark energy parametrizations (w CDM and CPL), and three viable $f(R)$ models (AB, HS, and ST). Our analyses employed MCMC methods to derive parameter constraints, quantified the impact of FRBs through the FoM in the (H_0, Ω_b) plane, and assessed model performance using AIC, BIC, and LRT statistics.

The inclusion of FRB data leads to significant improvements in cosmological constraints across all models. The most pronounced enhancements are observed in the baryon density Ω_b , with relative uncertainty reductions ranging from $\sim 25\%$ to $\sim 43\%$, with the largest gain in the CPL parametrization and the smallest in the ST model, confirming the nearly model-independent constraining power of the DM- z relation. For the Hubble constant H_0 , the improvement is more model-dependent, spanning $\sim 12\%$ to $\sim 35\%$, with the weakest gains in CPL and the strongest in viable $f(R)$ scenarios such as HS, reflecting the role of residual degeneracies. A similar pattern is observed for the absolute magnitude M_B , with reductions between $\sim 10\%$ and $\sim 32\%$, again showing diminished impact in CPL and stronger gains in models with tighter parameter correlations. Overall, these results highlight that FRBs

provide a robust constraint on Ω_b , while their impact on other parameters is mediated by the structure of model-dependent degeneracies.

Another common feature observed across all cosmological scenarios is a systematic upward shift in the mean values of both H_0 and Ω_b after the inclusion of FRB data. Although these shifts remain statistically consistent within the corresponding 1σ confidence intervals, they indicate that the FRB likelihood generally favors slightly larger expansion rates and baryon fractions. The effect is particularly pronounced in the Λ CDM and AB models, where the mean value of H_0 increases by $\sim 1.7 \text{ km s}^{-1} \text{ Mpc}^{-1}$, while Ω_b increases by ~ 0.003 .

In contrast, the matter density parameter Ω_m remains remarkably stable across most cosmological scenarios. Since its constraints are already dominated by geometric probes such as CC, SNe, and BAO observations, the additional information provided by FRBs generally has only a minor impact on its posterior distribution. A modest improvement is observed only in the CPL model, where the larger parameter space allows part of the FRB information to propagate into Ω_m .

For the additional parameters in the GR-based extensions, the inclusion of FRBs yields more limited benefits. In the w CDM case, w improves by $\sim 9\%$ and remains consistent with $w = -1$. In the CPL parametrization, (w_0, w_a) show uneven gains ($\sim 8\%$ and $\sim 22\%$, respectively), with w_a still weakly constrained. Although the marginal constraint on w_0 places $w_0 = -1$ outside the 68% confidence interval, the Λ CDM limit is not significantly disfavored, since $w_a = 0$ remains compatible with the data and the two-dimensional (w_0, w_a) constraints are considerably broader than the marginalized intervals. A qualitatively similar behavior has been reported in some DESI data combinations [59].

Similarly, in $f(R)$ models, only marginal improvements are obtained: only a lower bound on b could be established, while the uncertainties on μ_{HS} and λ_{S} decreased by $\sim 6\%$ and $\sim 15\%$, respectively, although the latter remains characterized by highly asymmetric uncertainties. No significant shifts were found in the central values of these parameters. Overall, these results indicate that FRBs have a limited impact on the additional degrees of freedom, with the constraints remaining largely dominated by parameter degeneracies.

The FRB nuisance parameters σ_{host} and e^μ exhibit only moderate variations across the different cosmological scenarios, with their inferred values remaining within relatively narrow ranges. This behavior suggests that these quantities are primarily determined by astrophysical properties of the host environment, with only a limited dependence on the underlying cosmological model. Consequently, the observed improvements in cosmological constraints appear to be driven mainly by the FRB cosmological information rather than by substantial shifts in the nuisance parameters.

The global impact of FRBs is quantified by the HPD-based FoM in the (H_0, Ω_b) plane, which increases by $\sim 48\%$ in Λ CDM case, $\sim 83\%$ in w CDM, and up to $\sim 91\%$ in CPL parametrization. This substantial enhancement is driven by the orthogonal constraint provided by the DM- z relation, which directly probes the integrated electron density and effectively breaks degeneracies between the expansion rate and the baryon content. Furthermore, FRBs induce a systematic reduction in parameter correlations and posterior skewness, leading to more Gaussian likelihood surfaces and more robust cosmological inferences.

The model comparison analysis reveals a moderate statistical preference for extensions beyond Λ CDM. Four alternative models, w CDM, CPL, HS, and ST, achieve improved fits to the data, reducing χ^2 by $|\Delta\chi^2| \approx 10$ relative to Λ CDM. Under the AIC, these models show strong evidence ($\Delta\text{AIC} < -7$), indicating that the improved fits compensate for the additional model complexity. However, the more conservative BIC penalizes the CPL model

due to its larger parameter space, retaining positive evidence only for w CDM, HS, and ST ($-3.2 < \Delta\text{BIC} < -2.7$). The LRT p -values, in turn, indicate an improvement over Λ CDM, with $p \sim 0.001\text{--}0.004$, corresponding to approximately 3σ statistical significance. However, this evidence should be interpreted with caution, as it remains well below the 5σ threshold typically required for a robust detection.

The comparable performance of w CDM and $f(R)$ models underscores a fundamental degeneracy. At the level of background observables, dark energy and modified gravity can produce nearly indistinguishable expansion histories. Since the probes employed in this work are primarily sensitive to $H(z)$ and geometric distances, they cannot decisively discriminate between these frameworks. Breaking this degeneracy requires the inclusion of perturbation-level observables that probe the growth of cosmic structure.

Future progress will require both larger datasets and complementary observables sensitive to structure formation. In particular, redshift-space distortions, weak gravitational lensing, the integrated Sachs-Wolfe effect, and cluster abundances provide information on the growth rate $f\sigma_8(z)$ and the metric potentials, which differ between dark energy and modified gravity even when their expansion histories are identical. The combination of these probes with an expanded FRB catalog will enable joint analyses that simultaneously constrain the expansion history, the baryon content, and the growth of structure.

For FRBs specifically, improvements in systematic control are essential. Current uncertainties are dominated by the modeling of the intergalactic medium ionization state, host galaxy contributions to the dispersion measure, and the precision of redshift measurements. As localization techniques improve and larger samples of FRBs with confirmed host galaxy associations become available, these systematic uncertainties are expected to decrease substantially. Refined theoretical models of the baryon distribution and improved calibration of the DM- z relation will enhance the cosmological constraining power of FRBs, especially at intermediate redshifts ($z \sim 0.5\text{--}1.5$), where current data are sparse.

Finally, this work demonstrates that FRBs may be a powerful and complementary probe of the cosmic baryon distribution, capable of significantly enhancing the constraining power of late-time cosmological datasets. While current data favor extensions beyond Λ CDM with moderate statistical significance, decisive discrimination between competing cosmological scenarios will require the combination of larger samples, improved systematic control, and the inclusion of observables sensitive to both background and perturbation dynamics.

Acknowledgments

B.W.N.R., L.L.S., K.E.L.F., R.A.B., and A.R.Q. thank the Paraíba State Research Foundation (FAPESQ) for financial support. A.R.Q. also acknowledges the support by CNPq under process number 310533/2022-8. K.E.L.F. and R.H.S. also thank CNPq for financial support.

A $f(R)$ Background Dynamics

In this appendix we outline the procedure used to determine the background expansion history $H(z)$ in $f(R)$ cosmology. The modified Friedmann equations (4.10) and (4.11) are recast into differential systems suitable for numerical integration, with formulations adapted to the specific structure of each model. In all cases, the ODE system is integrated forward in the scale factor from $a_i = 0.2$ to $a_f = 1.0$, corresponding to the redshift range $z \in [0, 4]$; the resulting solution is then mapped to $H(z)$ via the standard relation $a = (1 + z)^{-1}$. The initialization at

a_i is motivated by the fact that, for $z \gtrsim 4$, deviations from GR are strongly suppressed, so the background dynamics can be accurately approximated by the Λ CDM solution. The $H(z)$ profiles obtained in this way are subsequently used to construct a dense interpolation grid for efficient likelihood evaluations within the MCMC sampler.

Appleby-Battye model. For the AB model, the background dynamics can be expressed as a third-order ODE for the Hubble parameter as a function of the scale factor, $H(a)$. Adopting a as the independent variable and rewriting time derivatives via $\frac{d}{dt} = aH \frac{d}{da}$, the Ricci scalar takes the form

$$R = 6H (aH' + 2H), \quad (\text{A.1})$$

where primes denote derivatives with respect to a . Substituting this relation into the modified Friedmann equations (4.10) and (4.11), the system reduces to

$$H'''(a) = \mathcal{F}(a, H, H', H''), \quad (\text{A.2})$$

where \mathcal{F} encodes the full non-linear dependence on $f(R)$ and its derivatives. The third-order nature of this equation requires three initial conditions, set consistently with the Λ CDM background at a_i :

$$H_i \equiv H_{\Lambda\text{CDM}}(a_i), \quad H'_i \equiv H'_{\Lambda\text{CDM}}(a_i), \quad H''_i \equiv H''_{\Lambda\text{CDM}}(a_i). \quad (\text{A.3})$$

Hu-Sawicki and Starobinsky models. For the HS and ST models, we follow the strategy introduced in [10], which reformulate the background evolution in terms of the dimensionless variable $y_H(N)$, defined as $y_H \equiv (H^2/m^2) - a^{-3}$, where $N \equiv \ln a$ and $m^2 = H_0^2 \Omega_m$.

R^2 regularization. All three models include an R^2 regularization term whose role is to suppress high-frequency oscillations of the Ricci scalar and prevent the emergence of curvature singularities, while preserving the correct late-time cosmological behavior. The frequency of these small oscillations, $\omega_{\text{osc}} \equiv M_s \leq M$, depends on R and is therefore time-dependent. It is upper-bounded by the mass scale M , which is very large during inflation ($\sim 10^{13}$ GeV) and decreases as the universe ages. Following [49], an appropriate mass scale corresponds to $\delta_s \equiv \epsilon_{f(R)}/M^2 = 10^{-7}$ for the redshift range of interest ($0 \leq z \leq 4$). The characteristic curvature scale $\epsilon_{f(R)}$ takes model-specific values: ϵ_{AB} for the AB model, m^2 for the HS model, and R_S for the ST model.

Code availability. The numerical routines used to integrate the background equations for all models, along with the complete MCMC pipeline, are publicly available at <https://github.com/bwesley92/MCMC-cosmo>.

B CC and FRB Catalogs

This appendix lists the CC and FRB datasets described in Secs. 5 and 5, provided for completeness and reproducibility. The DESI DR2 BAO and Pantheon+ SNe Ia data are not reproduced here as they are publicly available from their respective collaborations.

z	$H(z)$	$\sigma_H(z)$	Ref.	z	$H(z)$	$\sigma_H(z)$	Ref.
0.07	69.0	19.6	[79]	0.593	104.0	13.0	[80]
0.09	69.0	12.0	[81]	0.68	92.0	8.0	[80]
0.12	68.6	26.2	[79]	0.75	98.8	33.6	[82]
0.17	83.0	8.0	[81]	0.75	105.0	7.9	[83]
0.179	75.0	4.0	[80]	0.781	105.0	12.0	[80]
0.199	75.0	5.0	[80]	0.8	113.1	15.1	[84]
0.2	72.9	29.6	[79]	0.875	125.0	17.0	[80]
0.27	77.0	14.0	[81]	0.88	90.0	40.0	[85]
0.28	88.8	36.6	[79]	0.9	117.0	23.0	[81]
0.352	83.0	14.0	[80]	1.037	154.0	20.0	[80]
0.3802	83.0	13.5	[86]	1.26	135.0	65.0	[87]
0.4	95.0	17.0	[81]	1.3	168.0	17.0	[81]
0.4004	77.0	10.2	[86]	1.363	160.0	33.6	[88]
0.4247	87.1	11.2	[86]	1.43	177.0	18.0	[81]
0.4497	92.8	12.9	[86]	1.53	140.0	14.0	[81]
0.47	89.0	49.6	[89]	1.75	202.0	40.0	[81]
0.4783	80.9	9.0	[86]	1.965	186.5	50.4	[88]
0.48	97.0	62.0	[85]				

Table 11. Catalog of 35 $H(z)$ measurements from CC, spanning $0.07 \leq z \leq 1.965$, compiled from multiple observational studies. Values are expressed in units of $\text{km s}^{-1} \text{Mpc}^{-1}$ with 1σ uncertainties.

Table 12: Catalog of 104 FRBs with measured DM_{obs} , redshifts, and identified host galaxies, covering the redshift range $0.0085 \leq z \leq 1.354$, compiled from multiple surveys and follow-up observations.

Name	z	$\text{DM}_{\text{obs}}(z)$	$\text{DM}_{\text{MW,ISM}}(z)$	Host	Ref.
FRB 20200723B	0.0085	244.0	33.0	3	[90]
FRB 20231229A	0.019	198.5	65.13	3	[60]
FRB 20240210A	0.0237	283.73	28.7	3	[61]
FRB 20231230A	0.0298	131.4	32.23	3	[60]
FRB 20181223C	0.0302	111.61	19.9	3	[64]
FRB 20240201A	0.0427	374.5	38.6	3	[61]
FRB 20220207C	0.0430	262.38	76.1	3	[63]
FRB 20211127I	0.0469	234.83	42.5	3	[65]
FRB 20200223B	0.0602	201.8	45.6	2	[69]
FRB 20190303A	0.064	223.2	29.8	2	[68]
FRB 20231204A	0.0644	221.0	34.94	2	[60]
FRB 20231206A	0.0659	457.7	37.51	3	[60]
FRB 20231120A	0.07	438.9	43.8	3	[62]
FRB 20190418A	0.0713	182.78	70.2	3	[64]
FRB 20211212A	0.0715	206.0	27.1	3	[65]
FRB 20231123A	0.0729	302.1	37.11	3	[60]

Continued on next page

Name	z	$DM_{\text{obs}}(z)$	$DM_{\text{MW,ISM}}(z)$	Host	Ref.
FRB 20231011A	0.0783	186.3	58.55	3	[60]
FRB 20220509G	0.0894	269.53	55.6	3	[63]
FRB 20230930A	0.0925	456.0	70.0	3	[91]
FRB 20230124A	0.0939	590.57	38.6	3	[62]
FRB 20201124A	0.098	413.52	139.9	2	[70]
FRB 20230708A	0.105	411.51	60.3	3	[61]
FRB 20191106C	0.1078	332.2	25.0	2	[69]
FRB 20231128A	0.1079	331.6	64.74	1	[60]
FRB 20230222B	0.11	187.8	57.0	3	[60]
FRB 20220914A	0.1139	631.28	54.7	3	[63]
FRB 20190608B	0.1178	338.7	37.3	3	[92]
FRB 20230703A	0.1184	291.3	38.16	3	[60]
FRB 20240213A	0.1185	357.4	40.0	3	[29]
FRB 20230222A	0.1223	706.1	33.31	3	[60]
FRB 20190110C	0.1224	221.6	37.1	2	[69]
FRB 20230628A	0.1265	344.95	39.0	3	[62]
FRB 20240310A	0.127	601.8	30.1	3	[61]
FRB 20210807D	0.1293	251.3	121.2	3	[65]
FRB 20240114A	0.13	527.65	49.7	1	[93]
FRB 20240209A	0.1384	176.52	63.1	2	[94]
FRB 20210410D	0.1415	571.2	56.2	3	[25]
FRB 20230203A	0.1464	420.1	67.3	3	[60]
FRB 20231226A	0.1569	329.9	38.1	3	[61]
FRB 20230526A	0.157	361.4	31.9	3	[61]
FRB 20220920A	0.1582	314.99	39.9	3	[63]
FRB 20200430A	0.1608	380.1	27.2	3	[66]
FRB 20210603A	0.1772	500.15	39.5	3	[23]
FRB 20220529A	0.1839	246.0	40.0	1	[24]
FRB 20230311A	0.1918	364.3	67.24	3	[60]
FRB 20220725A	0.1926	290.4	30.7	3	[61]
FRB 20121102A	0.1927	557.0	188.4	1	[16]
FRB 20221106A	0.2044	343.8	34.8	3	[61]
FRB 20240215A	0.21	549.5	47.9	3	[29]
FRB 20230730A	0.2115	312.5	114.65	3	[60]
FRB 20210117A	0.2145	729.1	34.4	3	[21]
FRB 20221027A	0.229	452.5	47.2	3	[62]
FRB 20191001A	0.234	506.92	44.2	3	[66]
FRB 20190714A	0.2365	504.13	38.5	3	[66]
FRB 20221101B	0.2395	491.55	131.2	3	[62]
FRB 20220825A	0.2414	651.24	78.5	3	[63]
FRB 20240304A	0.2423	652.6	73.9	3	[61]
FRB 20191228A	0.2432	297.5	32.9	3	[67]
FRB 20231017A	0.245	344.2	31.15	3	[60]
FRB 20221113A	0.2505	411.03	91.7	3	[62]

Continued on next page

Name	z	$DM_{\text{obs}}(z)$	$DM_{\text{MW,ISM}}(z)$	Host	Ref.
FRB 20220307B	0.2507	499.15	128.2	3	[63]
FRB 20231123B	0.2625	396.7	40.2	3	[62]
FRB 20230307A	0.271	608.9	37.6	3	[62]
FRB 20221116A	0.2764	643.45	132.3	3	[62]
FRB 20220105A	0.2785	583.0	22.0	3	[65]
FRB 20210320C	0.2797	384.8	39.3	3	[61]
FRB 20221012A	0.2847	441.08	54.3	3	[63]
FRB 20240229A	0.287	491.15	38.0	3	[29]
FRB 20190102C	0.2912	364.5	57.4	3	[20]
FRB 20220506D	0.3004	396.97	84.6	3	[63]
FRB 20230501A	0.301	532.5	125.6	3	[62]
FRB 20180924B	0.3214	361.42	40.5	3	[17]
FRB 20231025B	0.3238	368.7	65.58	3	[60]
FRB 20230626A	0.327	451.2	39.2	3	[62]
FRB 20180301A	0.3304	552.0	151.7	1	[67]
FRB 20231220A	0.3355	491.2	49.9	3	[29]
FRB 20211203C	0.3439	636.2	63.7	3	[65]
FRB 20230808F	0.3472	653.2	31.0	3	[95]
FRB 20220208A	0.351	437.0	101.6	3	[62]
FRB 20220726A	0.361	686.55	89.5	3	[62]
FRB 20230902A	0.3619	440.1	34.1	3	[61]
FRB 20220717A	0.363	637.34	118.3	3	[96]
FRB 20200906A	0.3688	577.8	35.8	3	[67]
FRB 20220330D	0.3714	468.1	38.6	3	[62]
FRB 20240119A	0.376	483.1	38.0	3	[29]
FRB 20190611B	0.3778	321.4	57.8	3	[66]
FRB 20220501C	0.381	449.5	30.6	3	[61]
FRB 20230506C	0.3896	772.0	68.0	2	[91]
FRB 20220204A	0.4012	612.58	50.7	3	[62]
FRB 20230712A	0.4525	587.57	39.2	3	[62]
FRB 20181112A	0.4755	589.27	41.7	3	[18]
FRB 20220310F	0.478	462.24	46.3	3	[63]
FRB 20220918A	0.491	656.8	153.1	3	[61]
FRB 20190711A	0.522	593.1	56.5	1	[66]
FRB 20230216A	0.531	828.0	38.5	3	[62]
FRB 20221219A	0.553	706.71	44.4	3	[62]
FRB 20230814A	0.553	696.4	104.8	3	[29]
FRB 20190614D	0.6	959.2	87.8	3	[63]
FRB 20220418A	0.622	623.25	36.7	3	[63]
FRB 20190523A	0.66	760.8	37.2	3	[19]
FRB 20240123A	0.968	1462.0	90.2	3	[29]
FRB 20221029A	0.975	1391.75	43.8	3	[62]
FRB 20220610A	1.016	1458.15	31.0	3	[22]
FRB 20220521B	1.354	1342.9	138.8	3	[61]

C Interpolation Grid Validation

For each $f(R)$ model, we validate the four-dimensional interpolation grid by comparing $H(z)$ obtained from direct ODE integration with the interpolated values at 300 random interior points drawn uniformly in the parameter space $(H_0, \Omega_m, \theta_{f(R)})$, excluding the outermost grid nodes to avoid boundary artifacts.

At each test point, we evaluate the relative interpolation error,

$$\Delta_H(z) = \left| \frac{H_{\text{interp}}(z) - H_{\text{ODE}}(z)}{H_{\text{ODE}}(z)} \right|, \quad (\text{C.1})$$

and record its maximum value over the redshift interval $z \in [0, 4]$. The resulting distribution of maximum errors is summarized in Table 13 through the median, the 95th percentile, and the global maximum.

Model	Median [%]	95th pct [%]	Max error [%]
AB	0.0062	0.0307	0.0492
HS	0.0053	0.0293	0.1029
ST	0.0055	0.0274	0.0503

Table 13. Summary of interpolation errors for $H(z)$ in each $f(R)$ model. Errors correspond to the distribution of the maximum relative deviation over $z \in [0, 4]$ evaluated at 300 random interior points.

All models satisfy the accuracy requirement adopted in Sec. 6.1, with maximum relative interpolation errors below 0.5% throughout the parameter space. When propagated to the observables at the data redshifts, the resulting deviations remain negligible compared to the observational uncertainties. The corresponding impact on the likelihood is entirely subdominant, with upper bounds on the induced shifts satisfying $\Delta\chi^2 \lesssim 3 \times 10^{-2}$ for all models and datasets. We therefore conclude that the interpolation procedure is numerically robust and does not affect the statistical inference or the model comparison results. Additional implementation details, validation tests, and numerical benchmarks are available in the public repository cited previously.

References

- [1] A.G. Riess, A.V. Filippenko, P. Challis, A. Clocchiatti, A. Diercks, P.M. Garnavich et al., *Observational evidence from supernovae for an accelerating universe and a cosmological constant*, *The Astronomical Journal* **116** (1998) 1009.
- [2] S. Perlmutter, G. Aldering, G. Goldhaber, R.A. Knop, P. Nugent, P.G. Castro et al., *Measurements of ω and λ from 42 high-redshift supernovae*, *The Astrophysical Journal* **517** (1999) 565.
- [3] S. Weinberg, *The cosmological constant problem*, *Reviews of Modern Physics* **61** (1989) 1.
- [4] E. Di Valentino, O. Mena, S. Pan, L. Visinelli, W. Yang, A. Melchiorri et al., *In the realm of the hubble tension—a review of solutions*, *Classical and Quantum Gravity* **38** (2021) 153001.
- [5] A.G. Riess, W. Yuan, L.M. Macri, D. Scolnic, D. Brout, S. Casertano et al., *A comprehensive measurement of the local value of the hubble constant with 1 km s⁻¹ mpc⁻¹ uncertainty from the hubble space telescope and the sh0es team*, *The Astrophysical Journal Letters* **934** (2022) L7.

- [6] L. Perivolaropoulos and F. Skara, *Challenges for λ cdm: An update*, *New Astronomy Reviews* **95** (2022) 101659.
- [7] M. Chevallier and D. Polarski, *Accelerating universes with scaling dark matter*, *International Journal of Modern Physics D* **10** (2001) 213–223.
- [8] E.V. Linder, *Exploring the expansion history of the universe*, *Physical Review Letters* **90** (2003) .
- [9] S.A. Appleby and R.A. Battye, *Do consistent models mimic general relativity plus λ ?*, *Physics Letters B* **654** (2007) 7.
- [10] W. Hu and I. Sawicki, *Models of $f(r)$ cosmic acceleration that evade solar system tests*, *Physical Review D* **76** (2007) .
- [11] A.A. Starobinsky, *Disappearing cosmological constant in $f(r)$ gravity*, *JETP Letters* **86** (2007) 157.
- [12] D.R. Lorimer, M. Bailes, M.A. McLaughlin, D.J. Narkevic and F. Crawford, *A bright millisecond radio burst of extragalactic origin*, *Science* **318** (2007) 777.
- [13] B. Zhang, *The physics of fast radio bursts*, *Reviews of Modern Physics* **95** (2023) .
- [14] THE CHIME/FRB collaboration, *The second chime/frb catalog of fast radio bursts*, *Astrophys. J. Suppl.* **283** (2026) 34 [2601.09399].
- [15] A. Hotan, J. Bunton, A. Chippendale, M. Whiting, J. Tuthill, V.A. Moss et al., *Australian square kilometre array pathfinder: I. system description*, *Publications of the Astronomical society of Australia* **38** (2021) e009.
- [16] S. Chatterjee, C.J. Law, R.S. Wharton, S. Burke-Spolaor, J.W.T. Hessels, G.C. Bower et al., *A direct localization of a fast radio burst and its host*, *Nature* **541** (2017) 58–61.
- [17] K.W. Bannister et al., *A single fast radio burst localized to a massive galaxy at cosmological distance*, *Science* **365** (2019) 565.
- [18] J.X. Prochaska, J.-P. Macquart, M. McQuinn, S. Simha, R.M. Shannon, C.K. Day et al., *The low density and magnetization of a massive galaxy halo exposed by a fast radio burst*, *Science* **366** (2019) 231–234.
- [19] V. Ravi, M. Catha, L. D’Addario, G. Djorgovski, G. Hallinan, R. Hobbs et al., *A fast radio burst localized to a massive galaxy*, *Nature* **572** (2019) 352.
- [20] S. Bhandari, K.W. Bannister, E. Lenc, H. Cho, R. Ekers, C.K. Day et al., *Limits on precursor and afterglow radio emission from a fast radio burst in a star-forming galaxy*, *The Astrophysical Journal Letters* **901** (2020) L20.
- [21] S. Bhandari, A.C. Gordon, D.R. Scott, L. Marnoch, N. Sridhar, P. Kumar et al., *A nonrepeating fast radio burst in a dwarf host galaxy*, *The Astrophysical Journal* **948** (2023) 67.
- [22] S.D. Ryder, K.W. Bannister, S. Bhandari, A.T. Deller, R.D. Ekers, M. Glowacki et al., *A luminous fast radio burst that probes the universe at redshift 1*, *Science* **382** (2023) 294–299.
- [23] T. Cassanelli, C. Leung, P. Sanghavi, J. Mena-Parra, S. Cary, R. Mckinven et al., *A fast radio burst localized at detection to an edge-on galaxy using very-long-baseline interferometry*, *Nature Astronomy* **8** (2024) 1429–1442.
- [24] Y. Li, S.B. Zhang, Y.P. Yang, C.W. Tsai, X. Yang, C.J. Law et al., *A sudden change and recovery in the magnetic environment around a repeating fast radio burst*, *Science* **391** (2026) 280–284.
- [25] M. Caleb, L.N. Driessen, A.C. Gordon, N. Tejos, L. Bernales, H. Qiu et al., *A subarcsec localized fast radio burst with a significant host galaxy dispersion measure contribution*, *Monthly Notices of the Royal Astronomical Society* **524** (2023) 2064–2077.

- [26] L.L. Sales, K.E.L. de Farias, A.R. Queiroz, J.R.L. Santos, R.A. Batista, A.R.M. Oliveira et al., *Cosmographic constraints from late-time probes including fast radio bursts*, *arXiv* (2025) [2507.06975].
- [27] T. Lemos, R.S. Gonçalves, J.C. Carvalho and J.S. Alcaniz, *Cosmological model-independent constraints on the baryon fraction in the igm from fast radio bursts and supernovae data*, *The European Physical Journal C* **83** (2023) .
- [28] J.-P. Macquart, J.X. Prochaska, M. McQuinn, K.W. Bannister, S. Bhandari, C.K. Day et al., *A census of baryons in the universe from localized fast radio bursts*, *Nature* **581** (2020) 391–395.
- [29] L. Connor et al., *A gas-rich cosmic web revealed by the partitioning of the missing baryons*, *Nature Astron.* **9** (2025) 1226 [2409.16952].
- [30] Y. Liu, J.-J. Wei, P. Wu and X.-F. Wu, *Dispersion measure distribution of unlocalized fast radio bursts as a probe of the hubble constant*, 2026.
- [31] I. Etherington, *Lx. on the definition of distance in general relativity*, *The London, Edinburgh, and Dublin Philosophical Magazine and Journal of Science* **15** (1933) 761.
- [32] A. Adame et al., *Desi 2024 vi: cosmological constraints from the measurements of baryon acoustic oscillations*, *Journal of Cosmology and Astroparticle Physics* **2025** (2025) 021.
- [33] N. Aghanim et al., *Planck 2018 results: Vi. cosmological parameters*, *Astronomy & Astrophysics* **641** (2020) A6.
- [34] E. Petroff, J.W.T. Hessels and D.R. Lorimer, *Fast radio bursts*, *The Astronomy and Astrophysics Review* **27** (2019) .
- [35] J.M. Cordes and T.J.W. Lazio, *NE2001. 1. A New model for the galactic distribution of free electrons and its fluctuations*, [astro-ph/0207156](#).
- [36] J.M. Shull, B.D. Smith and C.W. Danforth, *The baryon census in a multiphase intergalactic medium: 30% of the baryons may still be missing*, *The Astrophysical Journal* **759** (2012) 23.
- [37] J.-J. Wei, Z. Li, H. Gao and X.-F. Wu, *Constraining the evolution of the baryon fraction in the igm with frb and $h(z)$ data*, *Journal of Cosmology and Astroparticle Physics* **2019** (2019) 039–039.
- [38] J.-P. Dai and J.-Q. Xia, *Reconstruction of baryon fraction in intergalactic medium through dispersion measurements of fast radio bursts*, *Monthly Notices of the Royal Astronomical Society* **503** (2021) 4576–4580.
- [39] B. Wang and J.-J. Wei, *An 8.0% determination of the baryon fraction in the intergalactic medium from localized fast radio bursts*, *The Astrophysical Journal* **944** (2023) 50.
- [40] A.A. Meiksin, *The physics of the intergalactic medium*, *Reviews of Modern Physics* **81** (2009) 1405–1469.
- [41] G.D. Becker, J.S. Bolton, M.G. Haehnelt and W.L.W. Sargent, *Detection of extended he ii reionization in the temperature evolution of the intergalactic medium**, *Monthly Notices of the Royal Astronomical Society* **410** (2010) 1096–1112.
- [42] M. McQuinn, *Locating the “missing” baryons with extragalactic dispersion measure estimates*, *The Astrophysical Journal* **780** (2013) L33.
- [43] M. Jaroszynski, *Fast radio bursts and cosmological tests*, *Monthly Notices of the Royal Astronomical Society* **484** (2019) 1637–1644.
- [44] Z.J. Zhang, K. Yan, C.M. Li, G.Q. Zhang and F.Y. Wang, *Intergalactic medium dispersion measures of fast radio bursts estimated from illustrating simulation and their cosmological applications*, *The Astrophysical Journal* **906** (2021) 49.
- [45] D.-C. Qiang and H. Wei, *Reconstructing the fraction of baryons in the intergalactic medium with fast radio bursts via gaussian processes*, *Journal of Cosmology and Astroparticle Physics* **2020** (2020) 023–023.

- [46] G.Q. Zhang, H. Yu, J.H. He and F.Y. Wang, *Dispersion measures of fast radio burst host galaxies derived from illustrating simulation*, *The Astrophysical Journal* **900** (2020) 170.
- [47] T.P. Sotiriou and V. Faraoni, *f(r) theories of gravity*, *Reviews of Modern Physics* **82** (2010) 451–497.
- [48] A. De Felice and S. Tsujikawa, *f(r) theories*, *Living Reviews in Relativity* **13** (2010) .
- [49] S.A. Appleby, R.A. Battye and A.A. Starobinsky, *Curing singularities in cosmological evolution off(r) gravity*, *Journal of Cosmology and Astroparticle Physics* **2010** (2010) 005–005.
- [50] H. Motohashi and A. Nishizawa, *Reheating after f(r) inflation*, *Physical Review D* **86** (2012) .
- [51] A. Nishizawa and H. Motohashi, *Constraint on reheating after f(r) inflation from gravitational waves*, *Physical Review D* **89** (2014) .
- [52] B. Ribeiro, A. Bernui and M. Campista, *Cosmological constraints on the R²-corrected Appleby–Battye model*, *Eur. Phys. J. C* **84** (2024) 114 [2305.06392].
- [53] H. Motohashi, A.A. Starobinsky and J. Yokoyama, *Phantom boundary crossing and anomalous growth index of fluctuations in viable f(r) models of cosmic acceleration*, *Progress of Theoretical Physics* **123** (2010) 887–902.
- [54] R. Jimenez and A. Loeb, *Constraining cosmological parameters based on relative galaxy ages*, *The Astrophysical Journal* **573** (2002) 37–42.
- [55] A. Gómez-Valent, *Quantifying the evidence for the current speed-up of the universe with low and intermediate-redshift data. a more model-independent approach*, *Journal of Cosmology and Astroparticle Physics* **2019** (2019) 026–026.
- [56] Y. Yang and Y. Gong, *The evidence of cosmic acceleration and observational constraints*, *Journal of Cosmology and Astroparticle Physics* **2020** (2020) 059–059.
- [57] D. Scolnic, D. Brout, A. Carr, A.G. Riess, T.M. Davis, A. Dwomoh et al., *The pantheon+ analysis: The full data set and light-curve release*, *The Astrophysical Journal* **938** (2022) 113.
- [58] T.M. Davis, L. Hui, J.A. Frieman, T. Haugbølle, R. Kessler, B. Sinclair et al., *The effect of peculiar velocities on supernova cosmology*, *The Astrophysical Journal* **741** (2011) 67.
- [59] M. Abdul Karim et al., *Desi dr2 results. ii. measurements of baryon acoustic oscillations and cosmological constraints*, *Physical Review D* **112** (2025) .
- [60] CHIME/FRB collaboration, *A catalog of local universe fast radio bursts from chime/frb and the kko*, *Astrophys. J. Suppl.* **280** (2025) 6 [2502.11217].
- [61] R.M. Shannon, K.W. Bannister, A. Bera, S. Bhandari, C.K. Day, A.T. Deller et al., *The commensal real-time askap fast transient incoherent-sum survey*, *Publications of the Astronomical Society of Australia* **42** (2025) .
- [62] K. Sharma et al., *Preferential occurrence of fast radio bursts in massive star-forming galaxies*, *Nature* **635** (2024) 61 [2409.16964].
- [63] C.J. Law et al., *Deep Synoptic Array Science: First FRB and Host Galaxy Catalog*, *Astrophys. J.* **967** (2024) 29 [2307.03344].
- [64] M. Bhardwaj et al., *Host Galaxies for Four Nearby CHIME/FRB Sources and the Local Universe FRB Host Galaxy Population*, *Astrophys. J. Lett.* **971** (2024) L51 [2310.10018].
- [65] A.C. Gordon, W.-f. Fong, C.D. Kilpatrick, T. Eftekhari, J. Leja, J.X. Prochaska et al., *The demographics, stellar populations, and star formation histories of fast radio burst host galaxies: Implications for the progenitors*, *The Astrophysical Journal* **954** (2023) 80.
- [66] K.E. Heintz, J.X. Prochaska, S. Simha, E. Platts, W.-f. Fong, N. Tejos et al., *Host galaxy properties and offset distributions of fast radio bursts: Implications for their progenitors*, *The Astrophysical Journal* **903** (2020) 152.

- [67] S. Bhandari, K.E. Heintz, K. Aggarwal, L. Marnoch, C.K. Day, J. Sydnor et al., *Characterizing the fast radio burst host galaxy population and its connection to transients in the local and extragalactic universe*, *The Astronomical Journal* **163** (2022) 69.
- [68] D. Michilli, M. Bhardwaj, C. Brar, B.M. Gaensler, V.M. Kaspi, A. Kirichenko et al., *Subarcminute localization of 13 repeating fast radio bursts detected by chime/frb*, *The Astrophysical Journal* **950** (2023) 134.
- [69] A.L. Ibik et al., *Proposed Host Galaxies of Repeating Fast Radio Burst Sources Detected by CHIME/FRB*, *Astrophys. J.* **961** (2024) 99 [2304.02638].
- [70] V. Ravi, C.J. Law, D. Li, K. Aggarwal, M. Bhardwaj, S. Burke-Spolaor et al., *The host galaxy and persistent radio counterpart of frb 20201124a*, *Monthly Notices of the Royal Astronomical Society* **513** (2022) 982–990.
- [71] S. Yamasaki and T. Totani, *The galactic halo contribution to the dispersion measure of extragalactic fast radio bursts*, *The Astrophysical Journal* **888** (2020) 105.
- [72] A.M. Cook, M. Bhardwaj, B.M. Gaensler, P. Scholz, G.M. Eadie, A.S. Hill et al., *An frb sent me a dm: Constraining the electron column of the milky way halo with fast radio burst dispersion measures from chime/frb*, *The Astrophysical Journal* **946** (2023) 58.
- [73] L.C. Keating and U.-L. Pen, *Exploring the dispersion measure of the milky way halo*, *Monthly Notices of the Royal Astronomical Society: Letters* **496** (2020) L106–L110.
- [74] E. Platts, J.X. Prochaska and C.J. Law, *A data-driven technique using millisecond transients to measure the milky way halo*, *The Astrophysical Journal Letters* **895** (2020) L49.
- [75] Y. Liu, B. Wang, P. Wu, J.-J. Wei and X.-F. Wu, *Investigating the anisotropy of dispersion measure contribution from the galactic halo by using fast radio bursts*, *Astrophys. J.* **998** (2026) 15 [2601.02849].
- [76] A.C. Hindmarsh, *Odepack, a systematized collection of ode solvers*, in *Scientific Computing*, R.S.e.a. Stepleman, ed., (Amsterdam), pp. 55–64, North-Holland (1983).
- [77] F. Plaza and L. Kraiselburd, *Testing $f(r)$ -gravity models with desi dr2 2025-bao and other cosmological data*, *Physical Review D* **112** (2025) 023554.
- [78] S.S. Wilks, *The large-sample distribution of the likelihood ratio for testing composite hypotheses*, *The Annals of Mathematical Statistics* **9** (1938) 60.
- [79] C. Zhang, H. Zhang, S. Yuan, S. Liu, T.-J. Zhang and Y.-C. Sun, *Four new observational $h(z)$ data from luminous red galaxies in the sloan digital sky survey data release seven*, *Research in Astronomy and Astrophysics* **14** (2014) 1221.
- [80] M. Moresco, A. Cimatti, R. Jimenez, L. Pozzetti, G. Zamorani, M. Bolzonella et al., *Improved constraints on the expansion rate of the universe up to $z \sim 1.1$ from the spectroscopic evolution of cosmic chronometers*, *Journal of Cosmology and Astroparticle Physics* **2012** (2012) 006.
- [81] J. Simon, L. Verde and R. Jimenez, *Constraints on the redshift dependence of the dark energy potential*, *Phys. Rev. D* **71** (2005) 123001 [astro-ph/0412269].
- [82] N. Borghi, M. Moresco and A. Cimatti, *Toward a Better Understanding of Cosmic Chronometers: A New Measurement of $H(z)$ at $z \sim 0.7$* , *Astrophys. J. Lett.* **928** (2022) L4 [2110.04304].
- [83] R. Jimenez, M. Moresco, L. Verde and B.D. Wandelt, *Cosmic chronometers with photometry: a new path to $H(z)$* , *JCAP* **11** (2023) 047 [2306.11425].
- [84] K. Jiao, N. Borghi, M. Moresco and T.-J. Zhang, *New Observational $H(z)$ Data from Full-spectrum Fitting of Cosmic Chronometers in the LEGA-C Survey*, *Astrophys. J. Suppl.* **265** (2023) 48 [2205.05701].

- [85] D. Stern, R. Jimenez, L. Verde, M. Kamionkowski and S.A. Stanford, *Cosmic chronometers: constraining the equation of state of dark energy. i: $H(z)$ measurements*, *Journal of Cosmology and Astroparticle Physics* **2010** (2010) 008.
- [86] M. Moresco, L. Pozzetti, A. Cimatti, R. Jimenez, C. Maraston, L. Verde et al., *A 6% measurement of the Hubble parameter at $z \sim 0.45$: direct evidence of the epoch of cosmic re-acceleration*, *JCAP* **05** (2016) 014 [[1601.01701](#)].
- [87] E. Tomasetti, M. Moresco, N. Borghi, K. Jiao, A. Cimatti, L. Pozzetti et al., *A new measurement of the expansion history of the Universe at $z = 1.26$ with cosmic chronometers in VANDELS*, *Astron. Astrophys.* **679** (2023) A96 [[2305.16387](#)].
- [88] M. Moresco, *Raising the bar: new constraints on the Hubble parameter with cosmic chronometers at $z \sim 2$* , *Mon. Not. Roy. Astron. Soc.* **450** (2015) L16 [[1503.01116](#)].
- [89] A.L. Ratsimbazafy, S.I. Loubser, S.M. Crawford, C.M. Cress, B.A. Bassett, R.C. Nichol et al., *Age-dating luminous red galaxies observed with the southern african large telescope*, *Monthly Notices of the Royal Astronomical Society* **467** (2017) 3239–3254.
- [90] K. Shin et al., *Investigating the sightline of a highly scattered fast radio burst through a cosmic sheet structure in the local universe*, *Astrophys. J.* **993** (2025) 208 [[2410.07307](#)].
- [91] R. Anna-Thomas, C.J. Law, E.W. Koch, A.C. Gordon, K. Sharma, B.F. Williams et al., *Evidence for a hot galactic halo around the andromeda galaxy using fast radio bursts along two sightlines*, *The Astrophysical Journal* **993** (2025) 221.
- [92] J.S. Chittidi, S. Simha, A. Mannings, J.X. Prochaska, S.D. Ryder, M. Rafelski et al., *Dissecting the local environment of frb 190608 in the spiral arm of its host galaxy*, *The Astrophysical Journal* **922** (2021) 173.
- [93] J. Tian, K.M. Rajwade, I. Pastor-Marazuela, B.W. Stappers, M.C. Bezuidenhout, M. Caleb et al., *Detection and localization of the highly active FRB 20240114A with MeerKAT*, *Mon. Not. Roy. Astron. Soc.* **533** (2024) 3174 [[2408.10988](#)].
- [94] T. Eftekhari et al., *The Massive and Quiescent Elliptical Host Galaxy of the Repeating Fast Radio Burst FRB 20240209A*, *Astrophys. J. Lett.* **979** (2025) L22 [[2410.23336](#)].
- [95] K.Y. Hanmer, I. Pastor-Marazuela, J. Brink, D. Malesani, B.W. Stappers, P.J. Groot et al., *Contemporaneous optical-radio observations of a fast radio burst in a close galaxy pair*, *Monthly Notices of the Royal Astronomical Society* **538** (2025) 1800–1815.
- [96] K.M. Rajwade et al., *A study of two FRBs with low polarization fractions localized with the MeerTRAP transient buffer system*, *Mon. Not. Roy. Astron. Soc.* **532** (2024) 3881 [[2407.02173](#)].